Report
R-17-09
July 2017

Corrosion properties of cold worked or welded copper materials

Claes Taxén
Leyla Wickström
Mari Sparr

SVENSK KÄRNBRÄNSLEHANTERING AB

SWEDISH NUCLEAR FUEL
AND WASTE MANAGEMENT CO

Box 3091, SE-169 03 Solna
Phone +46 8 459 84 00
skb.se

SVENSK KÄRNBRÄNSLEHANTERING

ISSN 1402-3091
SKB R-17-09
ID 1571678
July 2017

Corrosion properties of cold worked or welded copper materials

Claes Taxén, Leyla Wickström, Mari Sparr
Swerea KIMAB AB

Summary

Copper for the manufacturing of canisters for nuclear waste was studied. First, the electrochemical behavior of cold worked copper from test rods previously subjected to various degrees of tensile or compressive strain was studied and compared to high purity copper without strain. Second, the electrochemical behavior of cold worked copper and friction stir welded copper was studied and compared to parent copper from the canister lid and to high purity copper. The surface morphology after forced corrosion was studied for the latter group of copper materials.

The results for the cold worked material from test rods indicate that the apparent nobility of the copper is independent of strain level, independent also of whether the strain is compressive or tensile and independent of whether the exposed surface is oriented along the strain or perpendicular to the strain. The test does not reveal any significant differences in apparent nobility between the weld, the parent material from the lid and the cold worked copper.

When forced electrochemically to corrode to an average depth of 40 μm, some small areas of the 0.2 cm^2 electrodes seem completely uncorroded. No areas where the corrosion had concentrated to more than double the average depth were found.

Contents

1 Background

Svensk Kärnbränslehantering AB (SKB) intends to use a phosphorous doped copper material in canisters for final deposition of spent nuclear fuel. The composition of the copper material is specified in SKB (2010), and is a highly pure copper (> 99.99 %) with a phosphorous addition of 30–100 ppm. In this investigation the electrochemical and corrosion behavior of phosphorous doped copper materials after various degrees of cold work is studied relative to a very pure copper material without cold work. Copper material from a friction stir weld is also included. The electrochemical properties studied are the equilibrium potential in copper containing solution and the surface morphology that arises when the material is forced to corrode electrochemically.

Galvanic corrosion studies between weld and base materials have previously been reported in Gubner and Andersson (2007).

2 Theory

In this study we investigate the apparent nobility of cold worked or welded copper material relative to very pure copper (without any cold work).

The apparent nobility is determined by measuring the equilibrium potentials of the materials when immersed in solutions with copper ions. Application of Nernst's law to the results allows estimation of the normal potential, E_0, for each material. Comparing experimentally determined values of E_0 for different copper materials should reveal differences in the activity of copper in these materials and hence differences in the driving force for corrosion. The theory is described in Taxén and Sparr (2014).

3 Material and electrodes

3.1 Cold worked copper from test rods

Three copper materials having been subjected to different degrees of cold worked were studied relative to a high purity copper without any cold work.

The three cold worked materials were taken from pieces of test rod from a test of mechanical creep (Andersson-Östling and Sandström 2009).

Test pieces were cut from parts of the test rods far from any visible crack.

The test pieces had labels identifying their history: “CuCW12-1”, “CuCW15-a” and “CuCW12-e”.

CuCW12-1: strained 12 % tensile.

CuCW15-a: strained 15 % compressive.

CuCW12-e: strained 12 % compressive.

3.2 Cold worked copper from a compressed copper barrel

Copper material from a compressed barrel was studied. A thick walled barrel was compressed 12 % in the axial direction (Andersson-Östling and Sandström 2009). From this, specimens were cut using Electric Discharge Machining. Further studies of the material is given in Wu et al. (2014).

Figure 3-1 shows photographs of the locations for where samples were taken for electrochemical measurements. The specimen labelled “CuCW12-e” in the previous section had been cut from the same compressed barrel.

Longitudinal samples were cut as cylinders with axes parallel to the axis of the compressed barrel and expose circular areas perpendicular to the direction of the strain. Transverse samples were cut as cylinders with axes perpendicular to the compressed barrel and expose circular areas along the strain, in one direction.

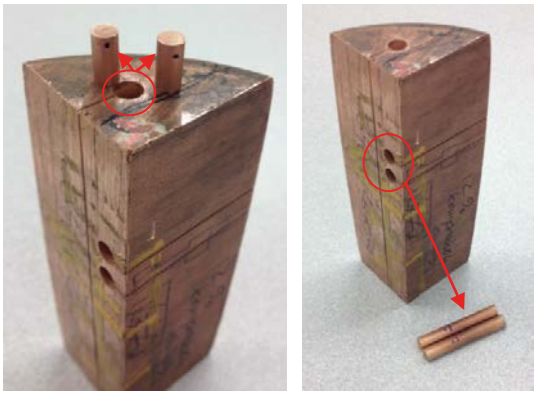

Figure 3-1. *Photographs of sample from a compressed copper barrel, indicating from where duplicate longitudinal (left) and duplicate transverse (right) specimens were cut.*

3.3 Welded copper and copper from a canister lid

Copper material from two places where a lid was friction stir welded to a copper canister were studied. Two samples were taken from the actual weld zone and two samples from the parent material of the lid. Figure 3-2 shows photographs of how the samples, with duplicates, were taken.

Longitudinal samples were cut as cylinders with axes parallel to that of the canister and expose circular areas parallel to the lid. Transverse samples were cut as cylinders with axes perpendicular to that of the canister and expose circular areas approximately perpendicular to the radius of the canister.

3.4 Electrodes

The electrode of high purity copper consisted of oblong balls or 'shots', Espi Metals, 6N purity. The cross section had elliptical shape with a major diameter of about 3 mm. The electrical connection was made by gluing a wire to the copper balls and a piece of copper sheet, using electrically conducting glue (Conductive Epoxy CW2400, Chemtronics). This arrangement was then cast in a resin (Epofix, Struers) so that only the high purity copper was exposed. Because of the small size of the copper balls, the exposed area was only approximately 7 mm^2. All copper electrodes were polished to 600 grit on SiC-paper.

3.4.1 Cold worked copper from test rods

Duplicate test specimens were cut from tensile test pieces which had been subjected to various degrees of stress, either by tensile or compressive loading. Figure 3-3 illustrates how sectioning of the test pieces was carried in two different orientations in relation to the applied tensile stresses. The orientation is analogous for samples subjected to compressive loading. The resulting test area was either rectangular (transverse) or half-circular (longitudinal) for the different orientations.

In order to make electrical contact with the copper samples, plastic sheathed wire (peeled at the ends) was fixed at the back of the specimens by conductive epoxy (Conductive Epoxy CW2400, Chemtronics). The samples were then cold mounted in a two component epoxy resin (Epofix, Struers). Each mount contained the duplicate samples (electrically insulated) from each material, i.e. 4 specimens/mount. Due to different dimensions of the tensile test samples, the resulting test pieces had slightly different dimensions and hence the surface area in contact with the solution varied between the specimens. The latter values have been specified in Table 3-1. The electrodes were labelled #1−16. The labelling is also clarified in Table 3-1.

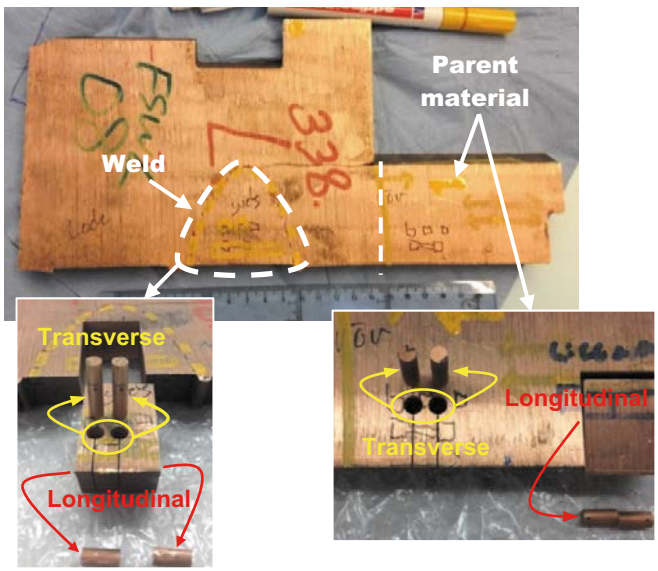

Figure 3-2. *Photographs of sample from copper canister lid, indicating where duplicate longitudinal and duplicate transverse specimens were cut from weld and parent material.*

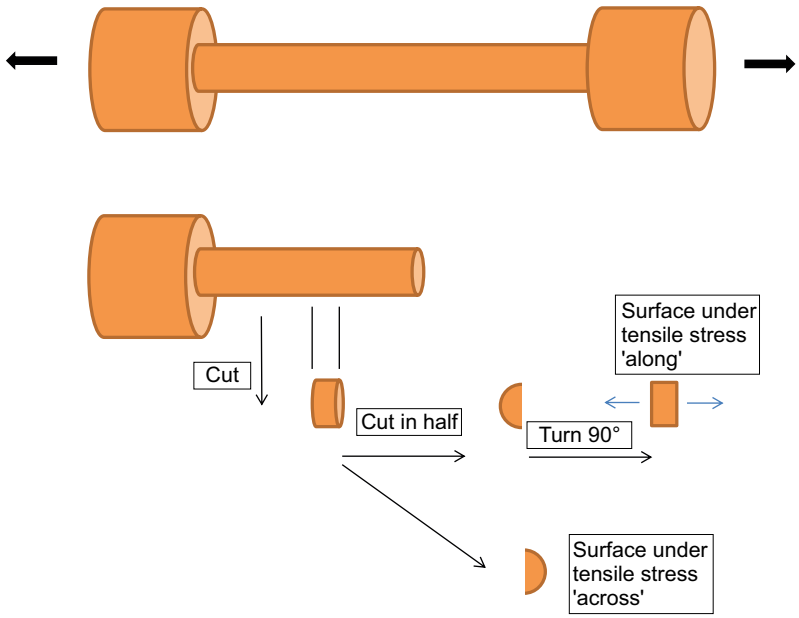

Figure 3-3. *Schematic illustration of how sectioning of test pieces was carried out from tensile samples and the resulting orientation of the test pieces in relation to the applied stress during cold work.*

Table 3-1. Electrode designations for the copper reference material and for samples from the test rods.

Electrode Number	Orientation with respect to stress direction	Electrode surface (cm^2)	Material
1	n/a	0.07	Reference copper
2	n/a		
3	n/a		
4	n/a		
5	Long (Cylind)	0.25	12 % tensile
6	Long (Cylind)		
7	Transv (Rect)	0.4	
8	Transv (Rect)		
9	Long (Cylind)	0.10	12 % compressive
10	Long (Cylind)		
11	Transv (Rect)	0.25	
12	Transv (Rect)		
13	Long (Cylind)	0.2	15 % compressive
14	Long (Cylind)		
15	Transv (Rect)	0.25	
16	Transv (Rect)		

All samples were cut as cylinders. Longitudinal samples expose circular areas perpendicular to the direction of the strain. Transverse samples expose rectangular areas along the strain, in one direction.

3.4.2 Cold worked copper from compressed barrel, copper from weld and from canister lid

In order to make electrical contact with the copper samples, plastic sheathed wire (peeled at the ends) was threaded through holes drilled at the ends of the cylinder specimens. The wire was eventually fixed to the specimens by conductive epoxy (Conductive Epoxy CW2400, Chemtronics). The samples were then cold mounted in a two component epoxy resin (Epofix, Struers). Each mount contained the duplicate samples, electrically insulated, from each material (longitudinal and transverse sections), i.e. 4 specimens/mount. Each cylinder had an area of approximately 0.2 cm^2 in contact with the solution.

The electrodes were labelled #1−16. The labelling is clarified in Table 3-2.

Table 3-2. Clarification of electrode designations for the copper reference material and for the samples from the copper canister.

Electrode Number	Orientation	Sample Material
1	n/a	Reference copper
2	n/a	
3	n/a	
4	n/a	
5	Transverse	Weld (lid)
6	Transverse	
7	Longitudinal	
8	Longitudinal	
9	Transverse	Core (canister)
10	Transverse	
11	Longitudinal	
12	Longitudinal	
13	Transverse	Parent (lid)
14	Transverse	
15	Longitudinal	
16	Longitudinal	

4 Experimental

4.1 Performance

Measurements of the cold worked copper from test rods are presented as runs #1 and #2. Measurements of the cold worked copper from the compressed barrel and from the weld are presented as run #3.

The experiments were carried out in a glass cell with a volume of approximately 1 L. A supporting electrolyte consisting of 0.5 M $MgSO_4$ at pH 2.5 was selected. This solution was selected to allow minor differences in the corrosion properties of the metal itself to manifest and not be clouded by solid corrosion products forming at the surface. Nitrogen gas was continuously bubbled through the test solution. The nitrogen gas came from the building's central gas system which is fed by nitrogen gas of quality Instrument 5.0, AGA. All additions during the course of the experiments were, however, made using solutions not previously de-aerated. The solution was stirred continuously (magnetic stirrer) throughout the duration of the test.

4.2 Equilibrium potentials for the copper materials

In order to measure how noble or un-noble the different copper materials behave, the electrodes' potential in solution were measured relative to a reference electrode of saturated calomel (SCE). All potentials are given relative to the SCE potential.

The copper content of the test solution was increased stepwise in order to verify that Nernst's law is applicable. Under conditions where Nernst's law is applicable the measurement of the electrode potentials gives a measure of the normal potential for the different copper materials.

The values of the normal potential, thus determined, are measurements of how noble the different copper materials behave relative to high purity copper. All potentials were measured using a potentiostat: Solartron Electrochemical Interface 1286. Before and after each experiment, the potential of the reference electrode was measured relative to a similar electrode that is always kept in saturated KCl. The difference was always less than 1 mV.

The copper content in the solution was increased by successive additions of a stock solution of 0.5 M $CuSO_4$ to the supporting electrolyte.

4.3 Surface morphology after forced corrosion

4.3.1 Forced corrosion

After the equilibrium potential measurements, accelerated corrosion was carried out for half of the duplicate electrodes from the different regions of the copper canister (6 electrodes in total) in 0.5 M $MgSO_4$ solution at pH 2.5. The electrodes were corroded simultaneously by applying a constant anodic current of 0.371 mA, in total. Based on an electrode area of approximately 0.2 cm^2/specimen, the average current density was 0.315 mA/cm^2 to each of the 6 electrodes. The time of the galvanostatic polarization was set to 96 hours so that the average corrosion depth would be 0.04 mm. The original intention was to corrode to an average depth of 0.10 mm. Due to a trivial calculation error the current density or time was set too low. The error was not discovered until after the electrical connections had been irrevocably cut from the electrodes.

A setup illustrated in Figure 4-1 was used to force six copper electrodes to corrode to an equal average depth. The potentio-galvanostat is set to deliver a certain constant current. The current branches to the separate electrodes. The resistance of the separate electrode may vary slightly but this resistance is much smaller than the resistance of the serial resistors. Thus an equal part of the current is forced through each electrode. Using 160 kΩ resistors, a voltage in the order of 10 V is required from the potentiostat in order to deliver the current to corrode an area of 0.2 cm^2 to an average depth of 0.04 mm in four days.

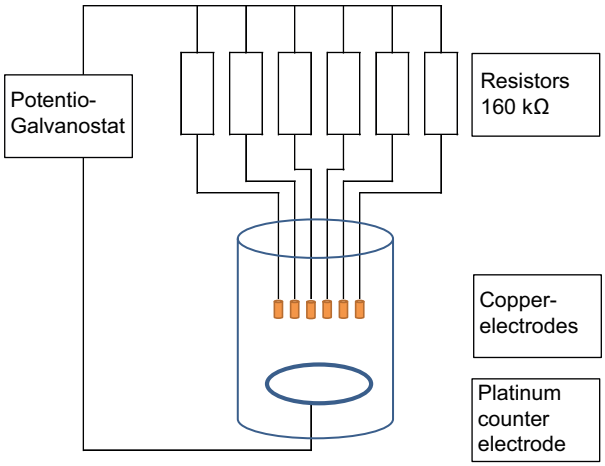

Figure 4-1. *Illustration of the setup used to forcibly corrode several copper electrodes simultaneously to the same average depth.*

4.3.2 Confocal microscopy

After forced corrosion to a certain average depth the electrodes were imaged by confocal microscopy in order to study the shape of the corrosion attack and the morphology of the surface.

4.4 Grain size distribution (optical microscopy)

After the equilibrium potential measurements, optical analysis of the cold worked copper specimens was carried out, in order to study any variation in grain size for the different orientations with respect to the applied stress.

Prior to analysis, the specimens were polished to a surface finish of 3 µm using diamond suspension followed by etching for 3−4 minutes in a solution consisting of 40 g CrO_3, 7.5 g NH_4Cl, 50 mL H_2SO_4 (95−97 %), 50 mL HNO_3 (65 %), 1 900 mL H_20.

5 Results

5.1 Equilibrium potentials for the copper materials

When potentials appeared stable, various additions of 0.5 M $CuSO_4$ were made to the solution in order to change the redox potential of the system. The potentials just prior to a change in the composition of the solution are here interpreted as the equilibrium potential of the electrode.

5.1.1 Cold worked copper from test rods

After initial measurements of the copper materials, some samples exhibited non-stable potentials. Closer examination of the electrodes (sample subjected to 15 % compressive strain) revealed cracks in the mount material immediately adjacent to the test surface of the electrodes. The cracks were sealed up by epoxy (Scotch Weld EC-9323 B/A) and the measurements were repeated. To prevent removal of the epoxy utilized to seal the cracks, no grinding was carried out of the electrode surfaces prior to the repeat measurements.

However, when run #2 was started the electrodes of the reference copper showed aberrant behaviour and the experiment was terminated. Some of the small pieces of the reference copper had an uneven, pitted appearance. The mount with the four electrodes of reference copper was gently repolished and the experiment was restarted.

The results from the separate experiments are presented as run #1 and run #2. No data from the interrupted first part of run #2 are presented.

Run #1

Figures 5-1, *a* through *d* and 5-2, *a* through *d* show the open circuit potential for the reference material and for the cold worked copper from test rods as function of experiment duration after run #1.

Table 5-1 shows a compilation of steady state values of the potential for the different copper electrodes at various solution compositions during run #1.

Figures 5-3, *a* through *d* and 5-4, *a* through *d* show the steady state values of the potential for the reference material and for the cold worked copper from test rods as function of the average potential of the four reference material electrodes.

Figures 5-5, *a* through *d* and 5-6, *a* through *d* show the steady state values of the potential, from Table 5-1 interpreted as equilibrium potentials, as function of the logarithm of the copper ion concentration. The solid lines in Figures 5-5 and 5-6 have the theoretical slope of 29.1 mV per decade. The legend in each graph shows the value of the estimated E_0. Data points corresponding to decreasing copper concentrations are omitted from Figures 5-5 and 5-6 because the dilution was not made with sufficient accuracy to correctly calculate the copper ion concentration.

Table 5-1. Steady state values of the electrode potentials for the different electrodes.

Time (Hours)	$[Cu^{2+}]$ (M)	Electrode Potential (mV SCE)															
		1	2	3	4	5	6	7	8	9	10	11	12	13	14	15	16
122	0.008	17.3	17.1	17.6	17.4	17.9	21.1	11.6	21.2	21.6	21.2	22.5	23.0	17.1	23.2	15.7	23.0
167	0.016	25.4	24.8	25.7	25.4	25.3	27.3	22.1	28.9	29.5	29.8	31.7	31.0	25.3	29.3	25.2	31.0
284	0.05	35.2	35.9	36.1	35.9	37.6	36.2	34.6	38.6	40.5	39.9	40.7	39.9	33.1	37.5	26.9	40.1
332	0.079	40.8	41.4	41.7	42.1	43.0	41.4	41.1	43.6	45.9	45.5	45.9	45.2	37.1	43.0	30.9	45.2
427	Dil. 1	28.4	27.1	28.1	28.8	33.0	33.1	33.4	31.8	34.1	33.8	33.1	34.2	27.9	31.1	24.6	33.2
456	Dil. 2	21.4	21.5	21.6	22.4	26.3	26.8	26.9	25.9	27.5	27.9	27.6	27.7	21.7	24.1	18.7	27.2
498	Dil. 3	15.6	14.3	15.5	16.2	19.8	20.7	20.4	19.6	21.3	21.3	21.0	21.4	15.4	18.4	10.0	20.9

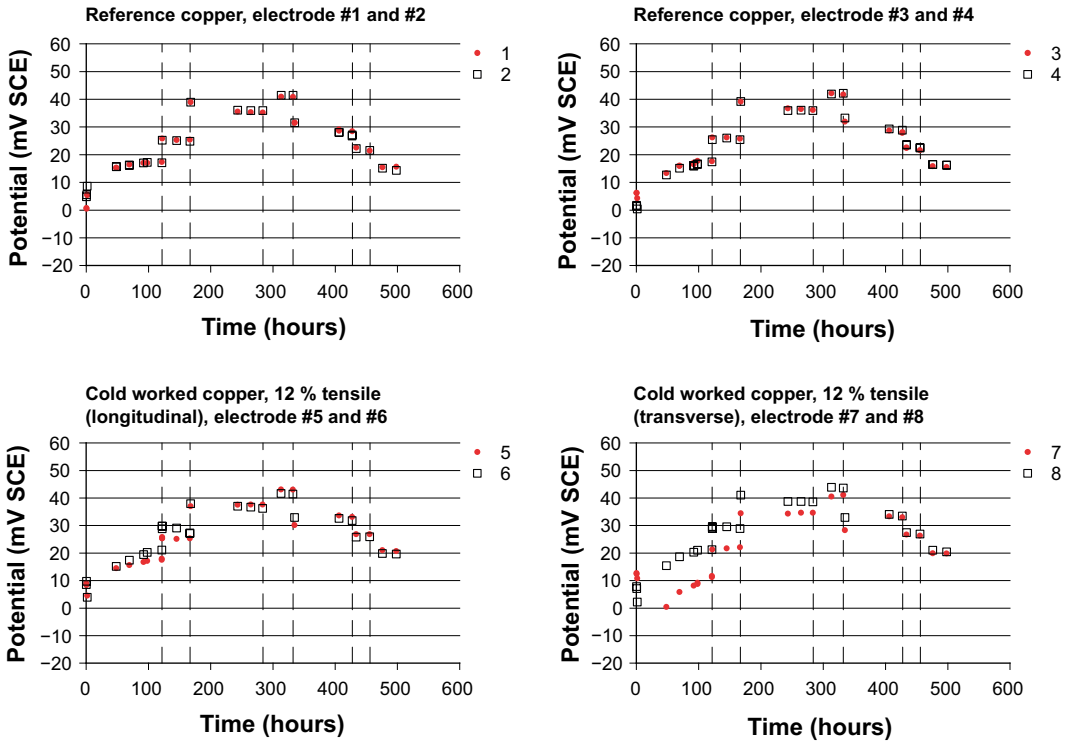

Figure 5-1. *Open circuit potentials for copper electrodes #1−8 (reference copper and cold worked copper) as function of experiment duration after run #1. The vertical dashed lines indicate times when the copper content in the solution was increased by the addition of a copper rich stock solution or decreased by dilution.*

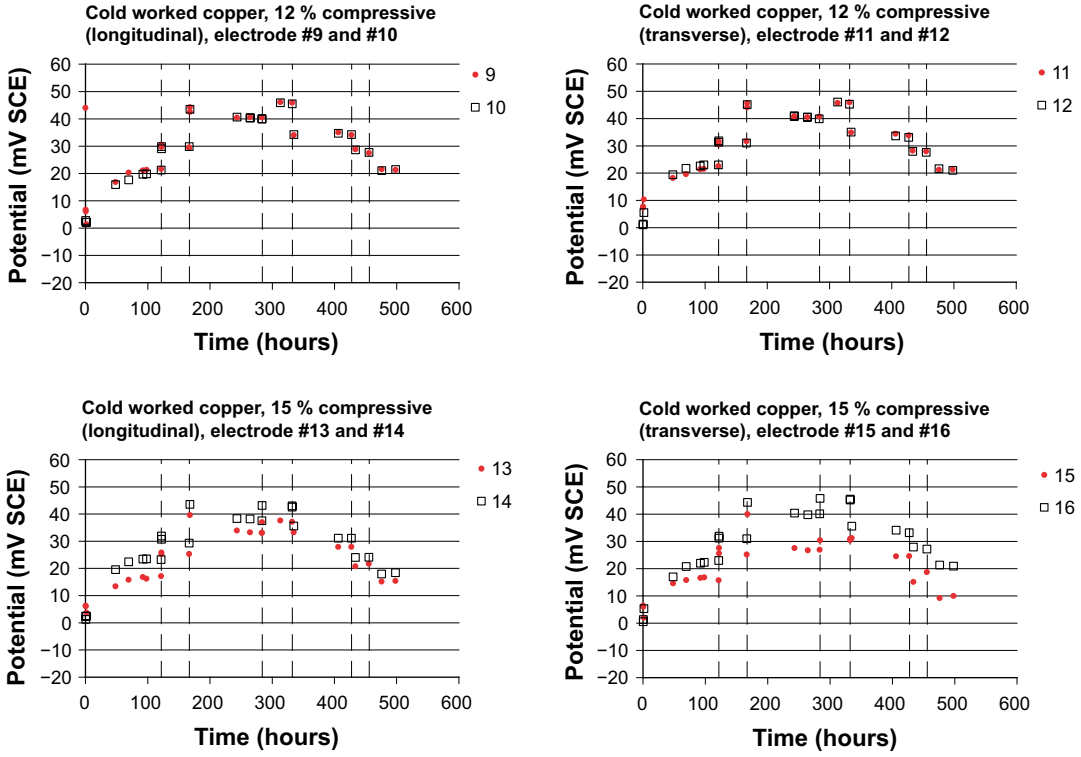

Figure 5-2. *Open circuit potentials for copper electrodes #9−16 (cold worked copper) as function of experiment duration after run #1. The vertical dashed lines indicate times when the copper content in the solution was increased by the addition of a copper rich stock solution or decreased by dilution.*

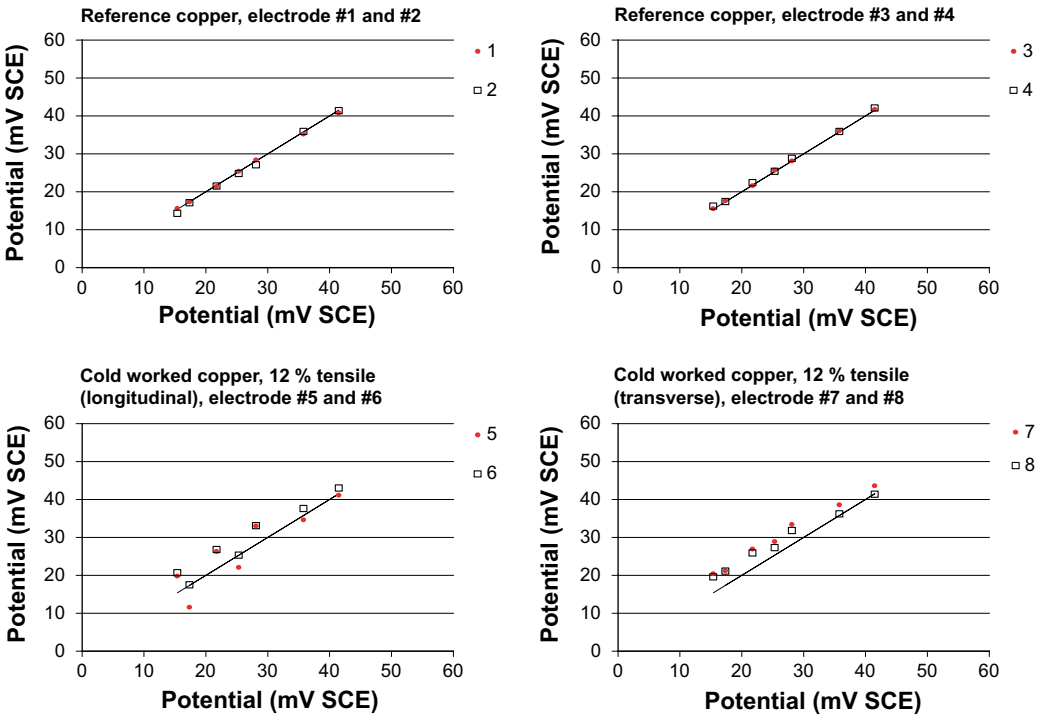

Figure 5-3. *Open circuit potentials for copper electrodes #1−8 (reference copper and cold worked copper) as function of the average potential of the reference material (electrodes #1−4) during run #1. The straight line shows the limit where the studied electrode behaves as more noble (over the straight line) and less noble (under the straight line) than the average of the four reference copper electrodes.*

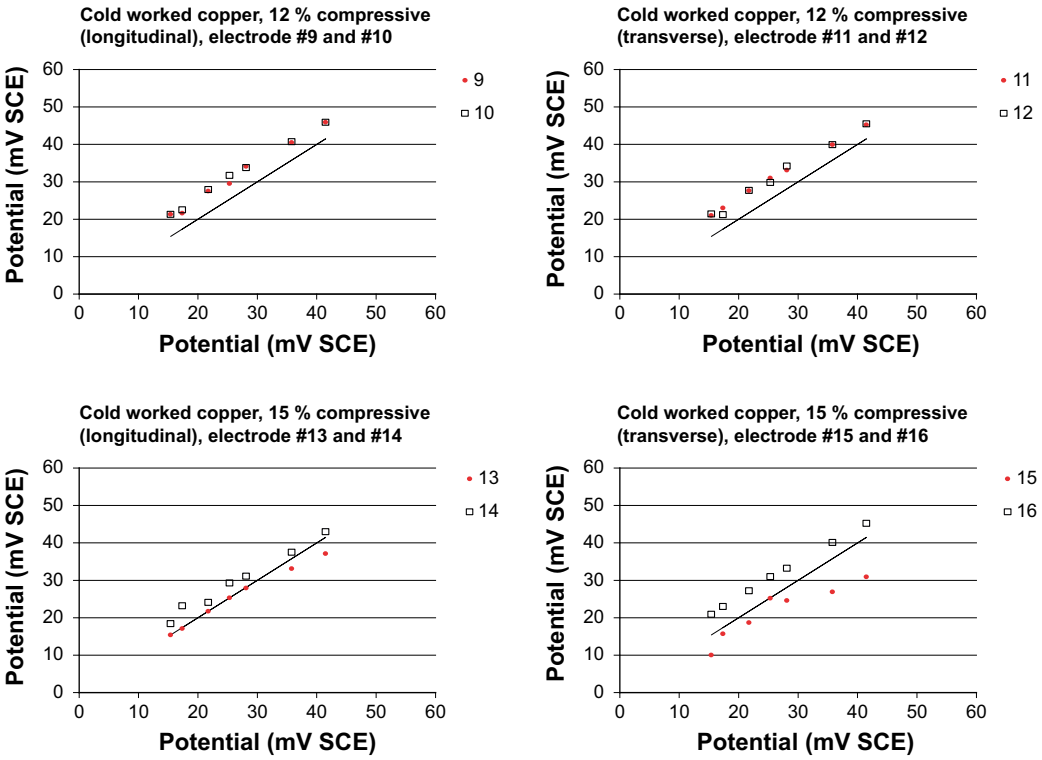

Figure 5-4. *Open circuit potentials for copper electrodes #9−16 (cold worked copper) as function of the average potential of the reference material (electrodes #1−4) during run #1. The straight line shows the limit where the studied electrode behaves as more noble (over the straight line) and less noble (under the straight line) than the average of the four reference copper electrodes.*

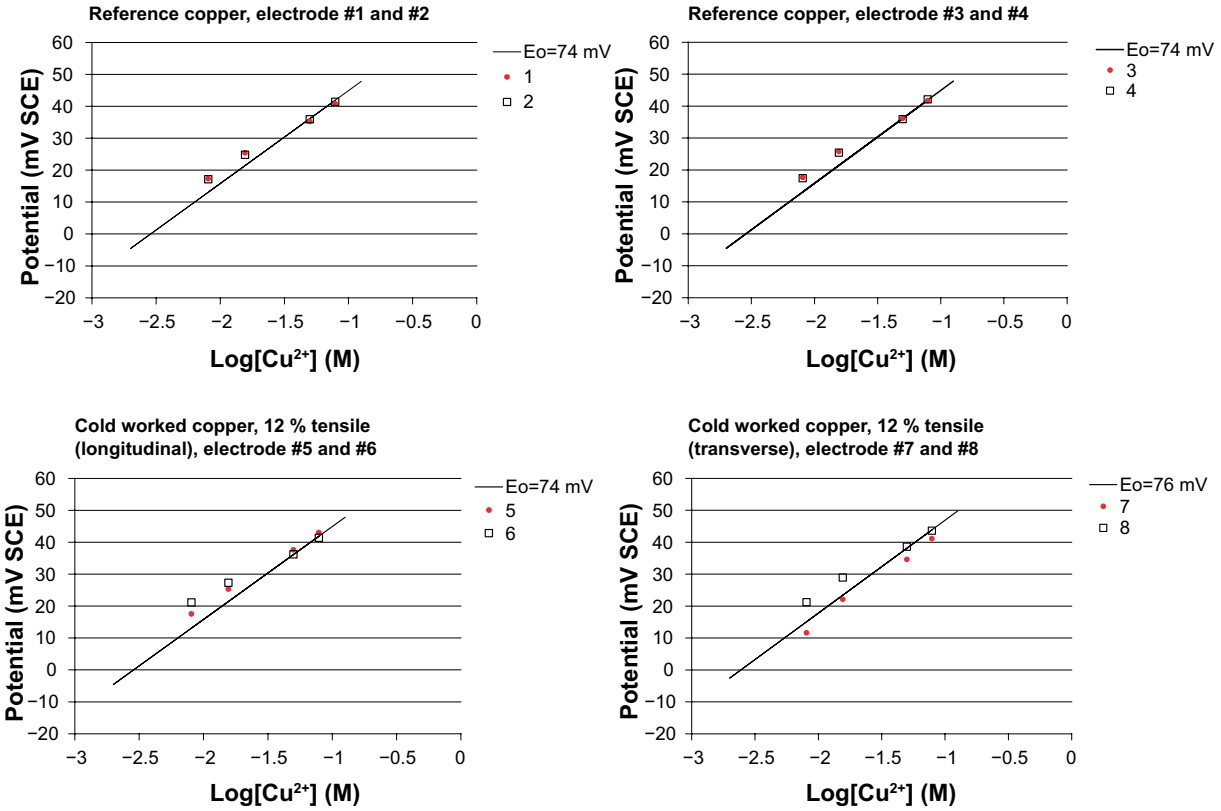

Figure 5-5. *Equilibrium potentials for copper electrodes #1−8 (reference copper and cold worked copper) as function of the logarithm of the copper ion concentration after run #1. The solid lines have the theoretical slope of 29.1 mV per decade. The legend in each graph shows the value of the estimated E_0.*

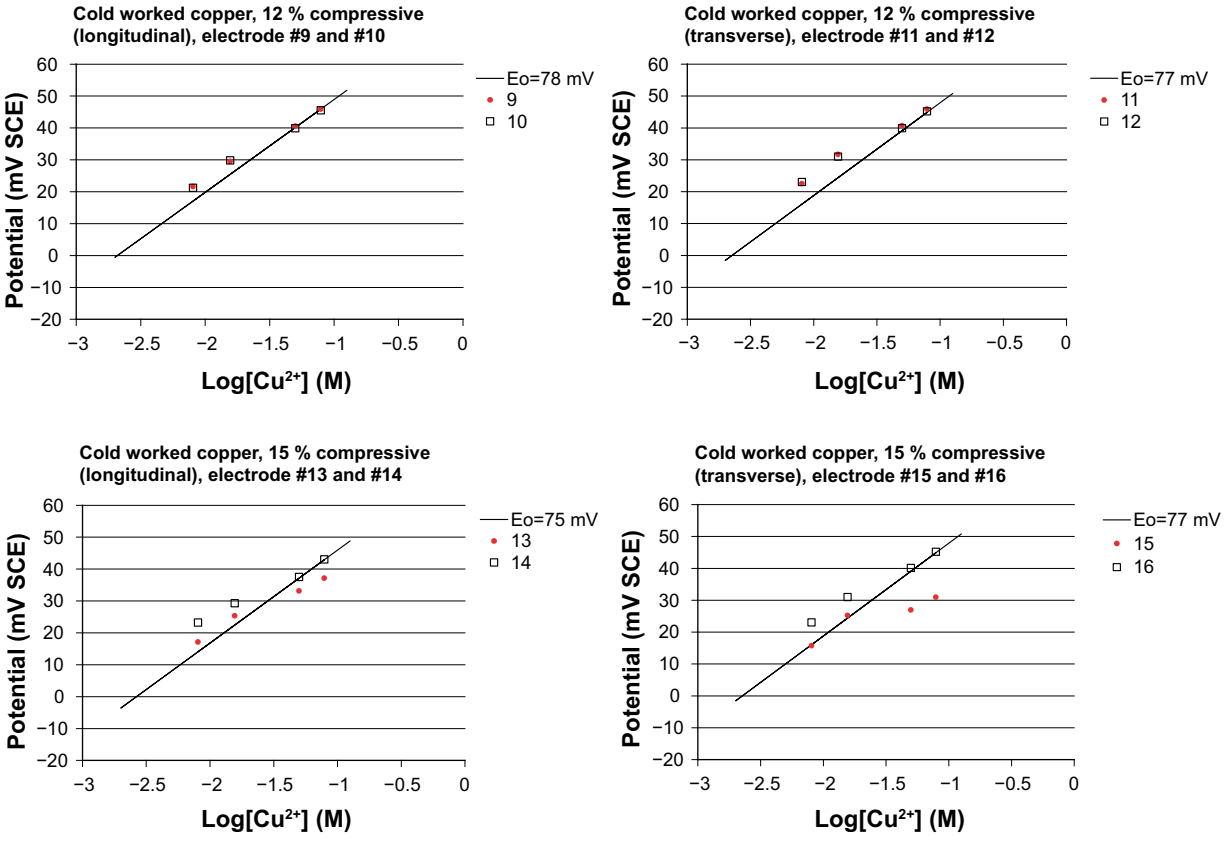

Figure 5-6. *Equilibrium potentials for copper electrodes #9−16 (cold worked copper) as function of the logarithm of the copper ion concentration after run #1. The solid lines have the theoretical slope of 29.1 mV per decade. The legend in each graph shows the value of the estimated E_0.*

Run #2

Figure 5-7, *a* through *d* and 5-8, *a* through *d* show the open circuit potential for the reference and cold worked copper as function of experiment duration.

Table 5-2 shows a compilation of steady state values of the potential for the different copper electrodes at various solution compositions.

Figures 5-9, *a* through *d* and 5-10, *a* through *d* show the steady state values of the potential for the reference material and for the cold worked copper from test rods as function of the average potential of the four reference material electrodes.

Figures 5-11, *a* through *d* and 5-12, *a* through *d* show the steady state values of the potential, from Table 5-2 interpreted as equilibrium potentials, as function of the logarithm of the copper ion concentration. The solid lines in Figures 5-11 and 5-12 have the theoretical slope of 29.1 mV per decade. The legend in each graph shows the value of the estimated E_0.

Table 5-2. Steady state values of the electrode potentials for the different electrodes.

Time (Hours)	$[Cu^{2+}]$ (M)	Electrode Potential (mV SCE)															
		1	**2**	**3**	**4**	**5**	**6**	**7**	**8**	**9**	**10**	**11**	**12**	**13**	**14**	**15**	**16**
64	0.02	30	29	28	32	34	35	35	34	36	36	36	36	33	34	35	35
164	0.037	35	35	34	37	37	39	38	39	42	42	42	42	41	39	40	39
260	0.068	38.7	37.2	37.6	40.6	43.2	44.3	43.3	44.1	46.3	47.0	46.7	46.3	45.8	45.5	46.2	45.6
359	0.095	42.4	41.7	41.0	43.4	48.5	49.0	48.1	48.9	49.7	50.7	50.1	50.3	51.0	50.5	51.2	50.7
502	0.011	14.4	13.4	13.8	15.1	17.5	17.5	16.7	17.3	20.3	20.3	20.2	20.5	20.0	18.8	19.4	19.3

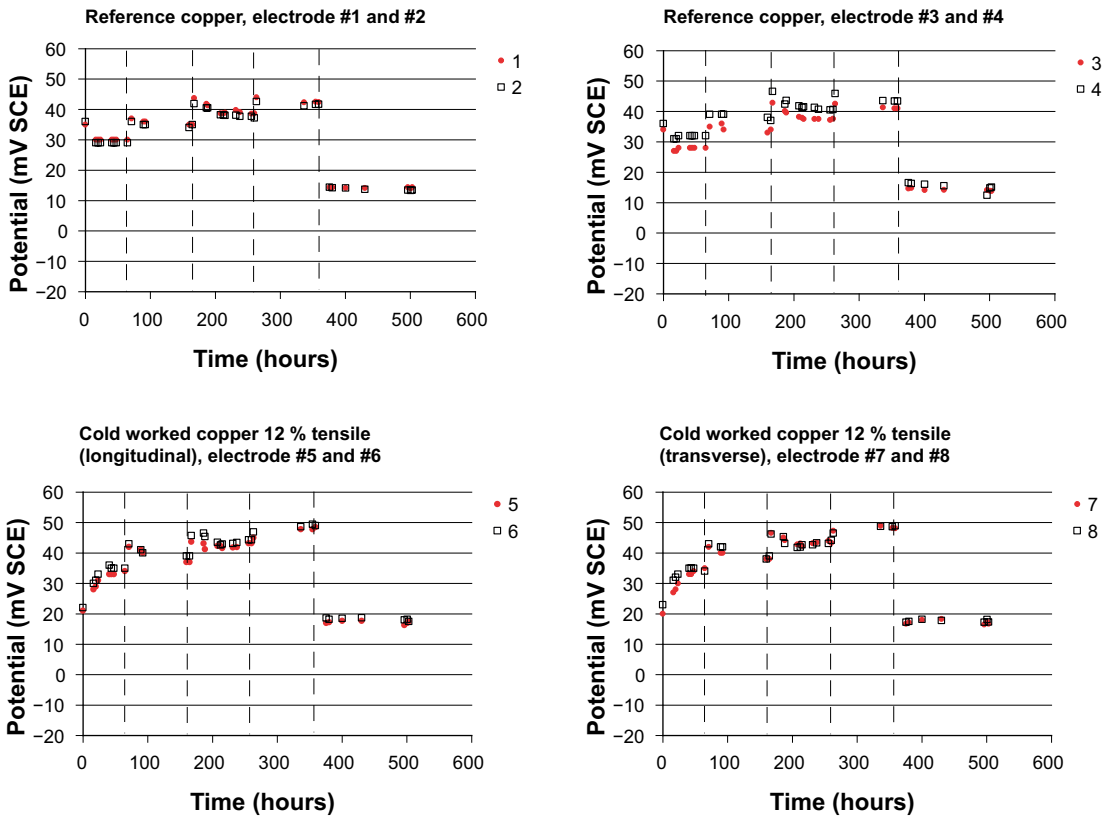

Figure 5-7. *Open circuit potentials for copper electrodes #1−8 (reference copper and cold worked copper) as function of experiment duration after run #2. The vertical dashed lines indicate times when the copper content in the solution was increased by the addition of a copper rich stock solution or decreased by dilution.*

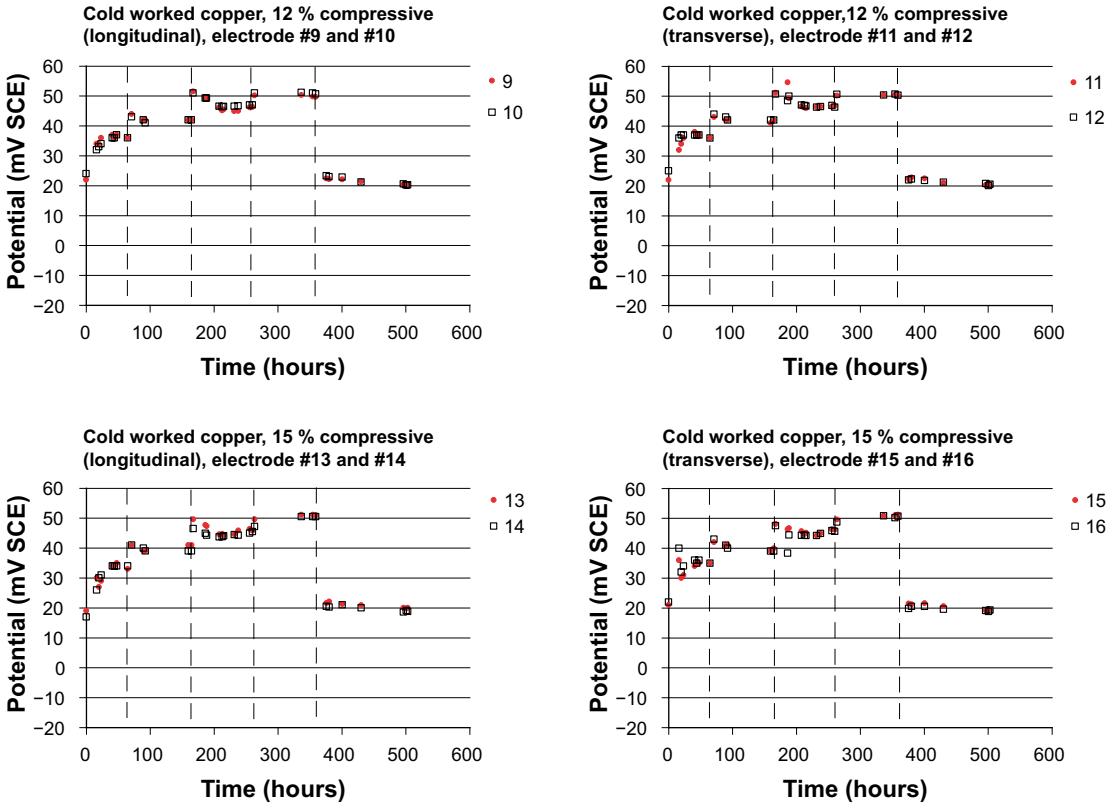

Figure 5-8. *Open circuit potentials for copper electrodes #9−16 (cold worked copper) as function of experiment duration after run #2. The vertical dashed lines indicate times when the copper content in the solution was increased by the addition of a copper rich stock solution.*

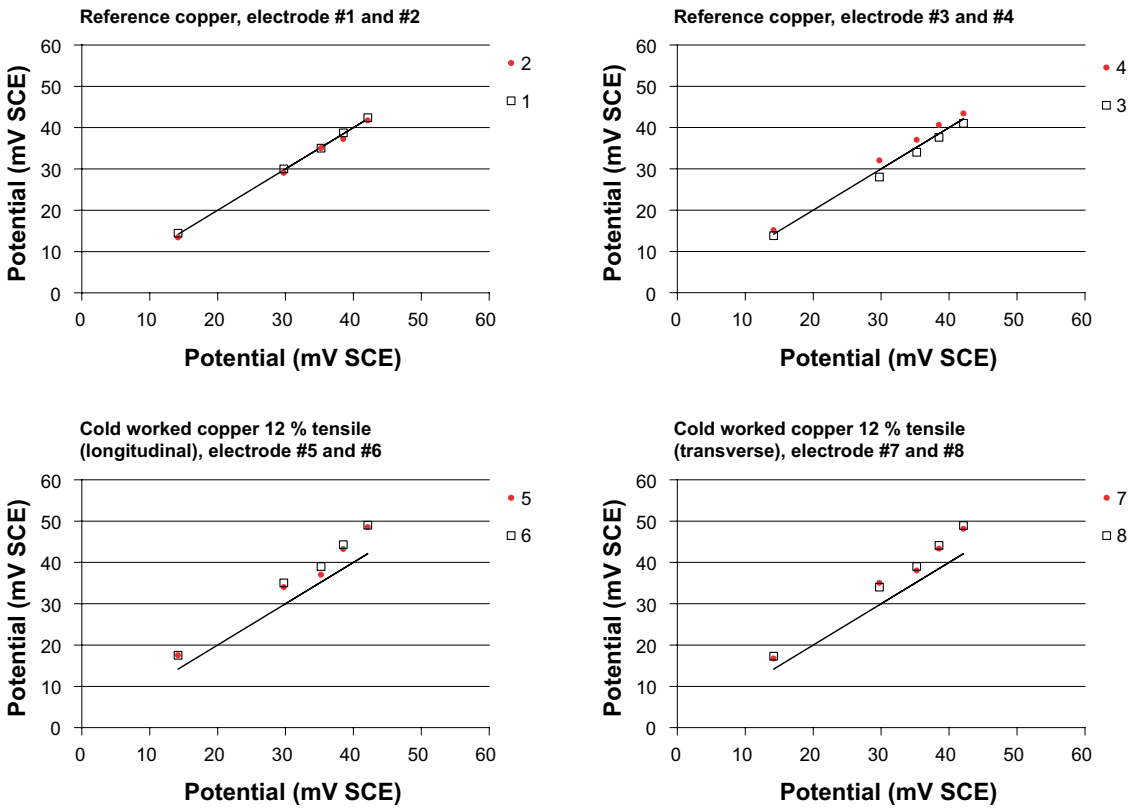

Figure 5-9. *Open circuit potentials for copper electrodes #1−8 (reference copper and cold worked copper) as function of the average potential of the reference material (electrodes #1−4) during run #2. The straight line shows the limit where the studied electrode behaves as more noble (over the straight line) and less noble (under the straight line) than the average of the four reference copper electrodes.*

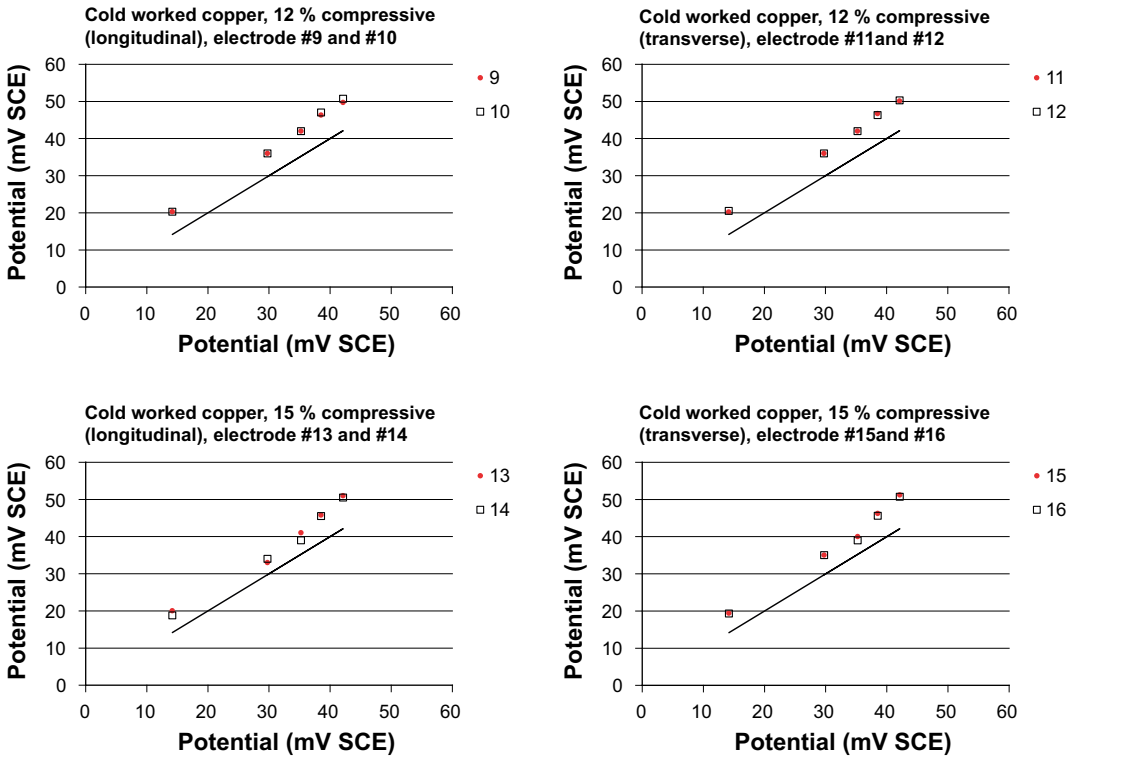

Figure 5-10. *Open circuit potentials for copper electrodes #9−16 (cold worked copper) as function of the average potential of the reference material (electrodes #1−4) during run #2. The straight line shows the limit where the studied electrode behaves as more noble (over the straight line) and less noble (under the straight line) than the average of the four reference copper electrodes.*

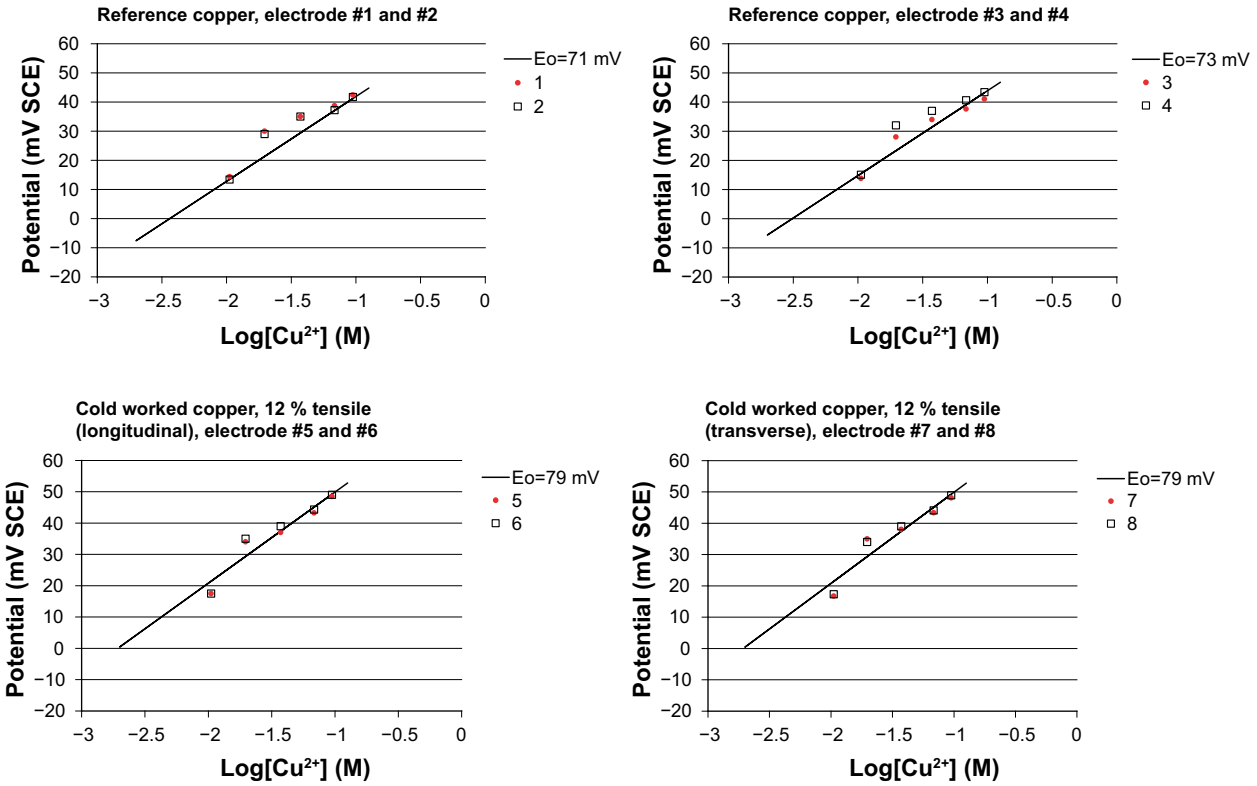

Figure 5-11. *Equilibrium potentials for copper electrodes #1−8 (reference copper and cold worked copper) as function of the logarithm of the copper ion concentration after run #2. The solid lines have the theoretical slope of 29.1 mV per decade. The legend in each graph shows the value of the estimated* E_0.

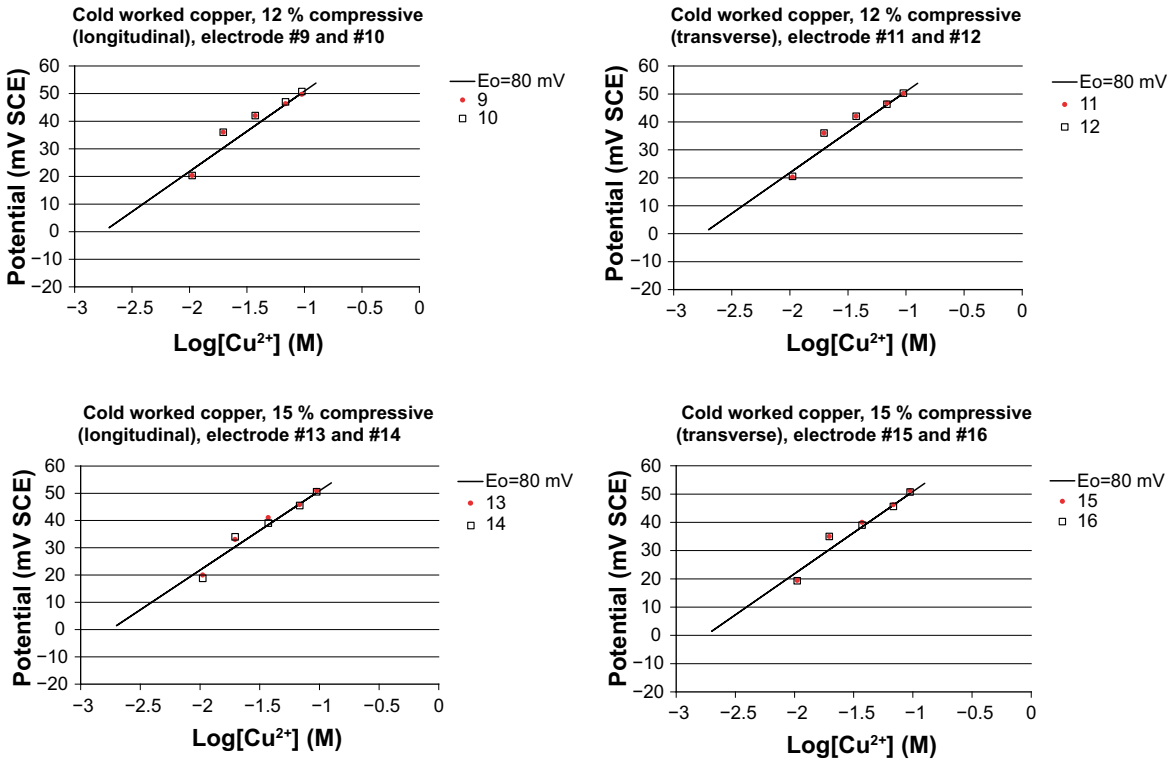

Figure 5-12. *Equilibrium potentials for copper electrodes #9−16 (cold worked copper) as function of the logarithm of the copper ion concentration after run #2. The solid lines have the theoretical slope of 29.1 mV per decade. The legend in each graph shows the value of the estimated* E_0.

5.1.2 Summary of results from runs #1 and #2

Table 5-3 summarizes the results for the copper materials from test rods in terms of the estimated normal potentials, E_0.

Table 5-3. Summary of results from electrode potential measurements of cold worked copper from test rods.

Electrode Number	Orientation with respect to stress direction	Material	E_0 values from Run #1	E_0 values from Run #2
1, 2	n/a	Reference copper	74	71
3, 4	n/a		74	73
5, 6	Long (Cylind)	12 % tensile	74	79
7, 8	Transv (Rect)		76	79
9, 10	Long (Cylind)	12 % compressive	78	80
11, 12	Transv (Rect)		77	80
13, 14	Long (Cylind)	15 % compressive	75	80
15, 16	Transv (Rect)		77	80

Data for electrode numbers 13 and 15 from run #1 were omitted from Table 5-3 since the potentials showed aberrant behaviour and the electrode mount material was found to be cracked near those electrodes.

5.1.3 Cold worked copper from compressed barrel, copper from weld and from canister lid

Figure 5-13, *a* through *d* and 5-14, *a* through *d* show the open circuit potential for the reference and copper canister samples as function of experiment duration.

Table 5-4 shows a compilation of steady state values of the potential for the different copper electrodes at various solution compositions.

Figures 5-15, *a* through *d* and 5-16, *a* through *d* show the steady state values of the potential for the reference material and for the cold worked copper from test rods as function of the average potential of the four reference material electrodes.

Figures 5-17, *a* through *d* and 5-18, *a* through *d* show the steady state values of the potential, from Table 5-4 interpreted as equilibrium potentials, as function of the logarithm of the copper ion concentration. The solid lines in Figures 5-17 and 5-18 have the theoretical slope of 29.1 mV per decade. The legend in each graph shows the value of the estimated E_0.

Table 5-4. Steady state values of the electrode potentials for the different electrodes.

Time (Hours)	$[Cu^{2+}]$ (M)	Electrode Potential (mV SCE)															
		1	2	3	4	5	6	7	8	9	10	11	12	13	14	15	16
117	0.02	18.3	15.1	14.6	14.7	22.1	23.7	22.9	22.7	23.1	25.3	23.5	25.1	21.9	22.7	22.8	23.1
214	0.037	18.6	20.9	23.6	21.9	29.9	30.0	30.1	29.6	31.7	31.1	31.0	33.1	29.0	28.9	31.4	31.1
357	0.068	22.6	24.9	27.8	26.8	34.5	36.8	33.8	34.0	35.7	35.8	35.5	36.7	34.5	32.7	33.1	34.2
526	0.095	28.2	30.4	31.2	29.5	41.0	41.3	40.4	36.1	40.5	39.4	38.4	42.5	38.9	37.0	36.4	37.5
718	0.032	20.0	17.5	19.6	17.4	25.1	25.8	21.5	18.2	25.4	25.9	23.5	27.5	25.1	24.7	25.4	23.4
1151	0.011	6.8	5.4	4.6	5.6	7.0	6.7	5.9	3.9	8.7	9.6	6.6	7.4	6.7	6.6	6.7	7.2

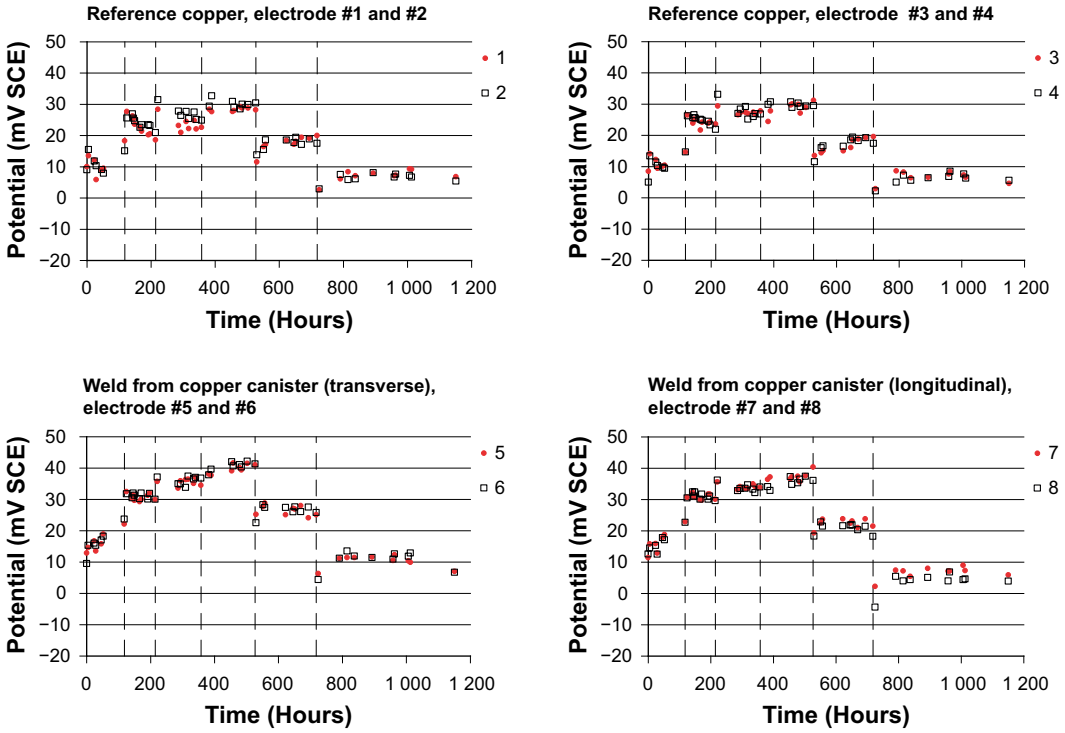

Figure 5-13. *Open circuit potentials for copper electrodes #1−8 (reference copper and copper from a weld) as function of experiment duration. The vertical dashed lines indicate times when the copper content in the solution was increased by the addition of a copper rich stock solution.*

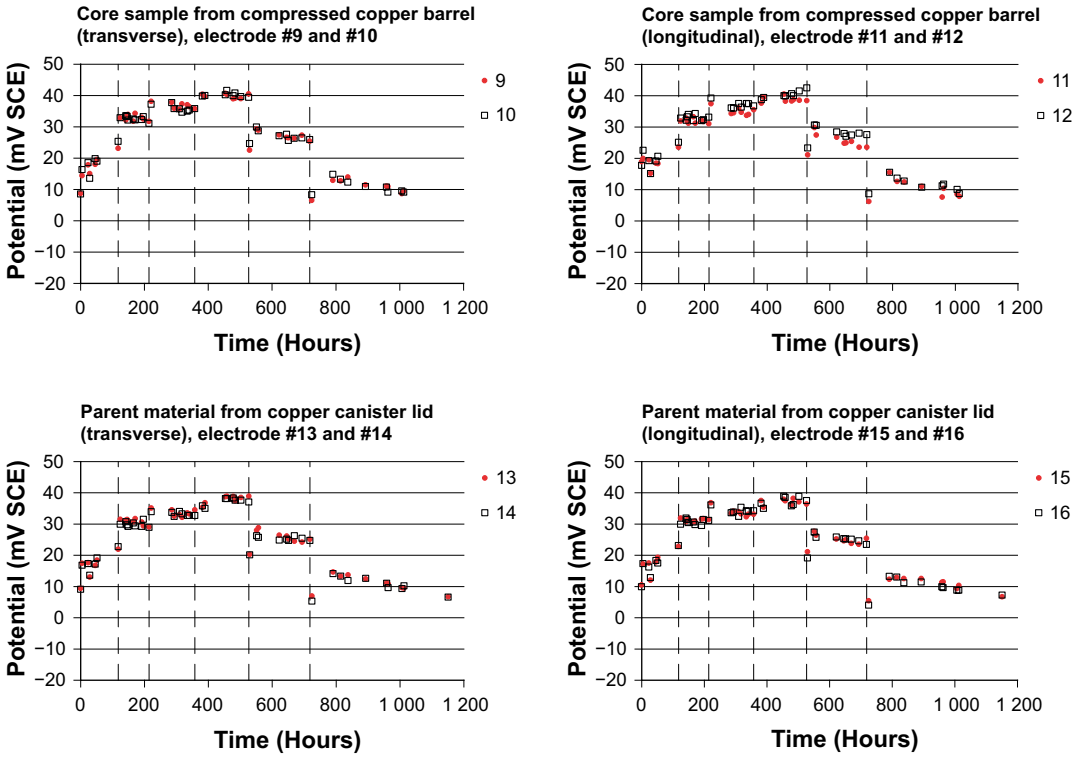

Figure 5-14. *Open circuit potentials for copper electrodes #9−16 (copper canister) as function of experiment duration. The vertical dashed lines indicate times when the copper content in the solution was increased by the addition of a copper rich stock solution or decreased by dilution.*

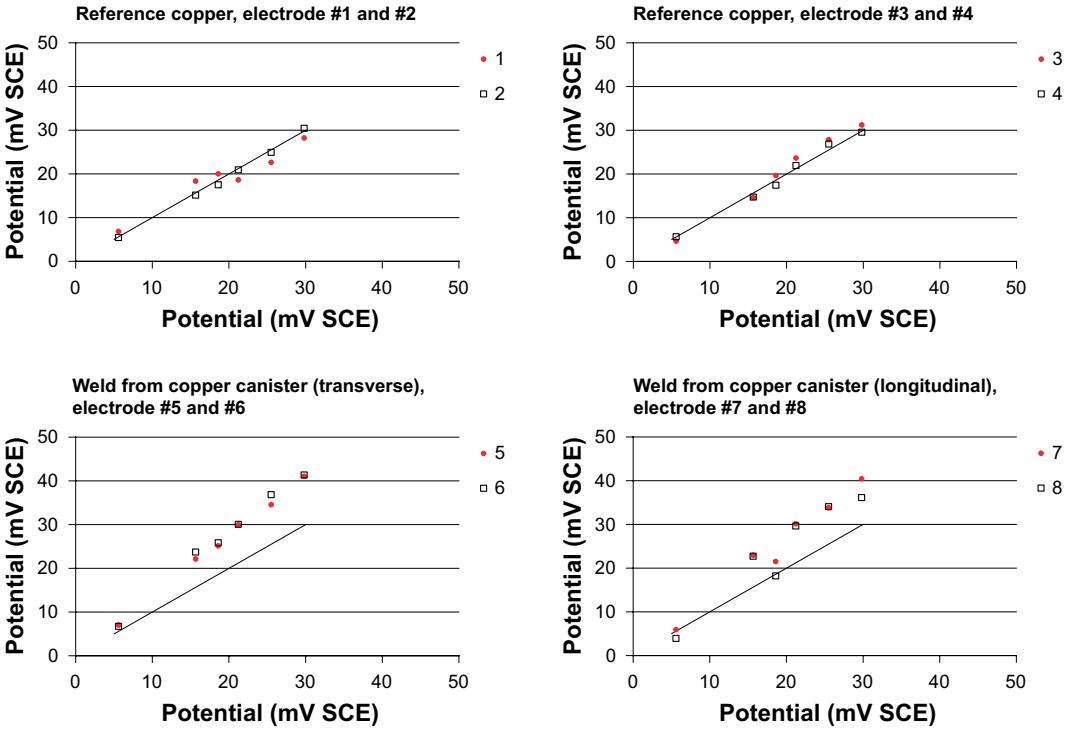

Figure 5-15. *Open circuit potentials for copper electrodes #1−8 (reference copper and cold worked copper) as function of the average potential of the reference material (electrodes #1−4). The straight line shows the limit where the studied electrode behaves as more noble (over the straight line) and less noble (under the straight line) than the average of the four reference copper electrodes.*

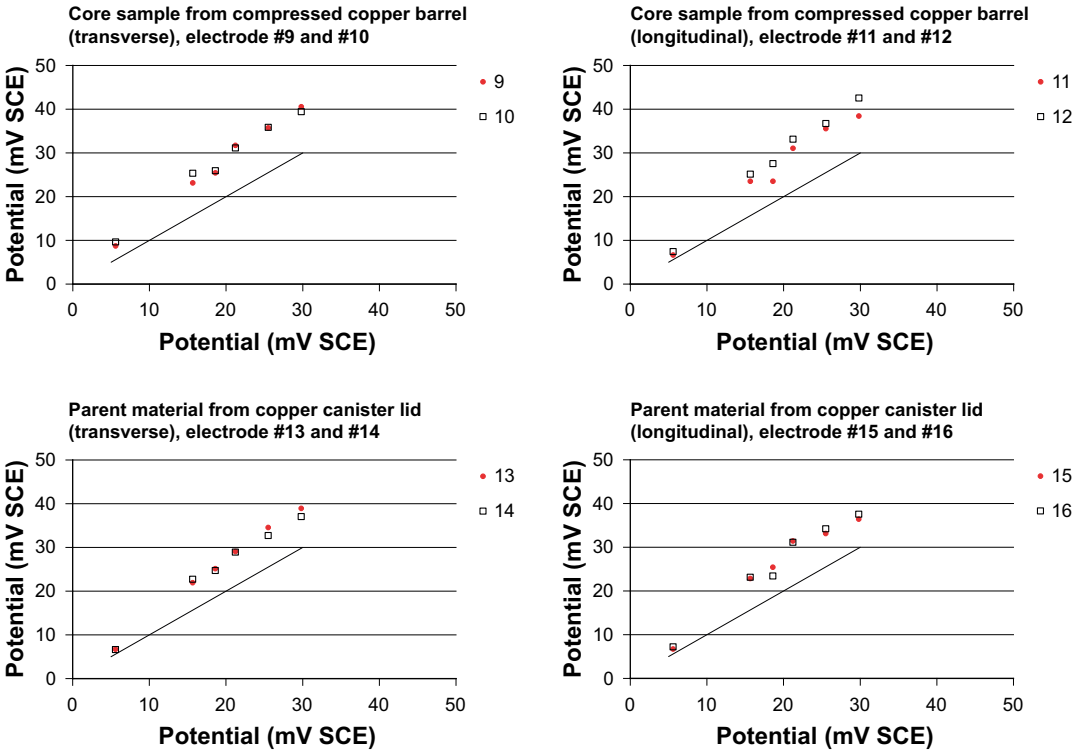

Figure 5-16. *Open circuit potentials for copper electrodes #9−16 (copper canister) as function of the average potential of the reference material (electrodes #1−4). The straight line shows the limit where the studied electrode behaves as more noble (over the straight line) and less noble (under the straight line) than the average of the four reference copper electrodes.*

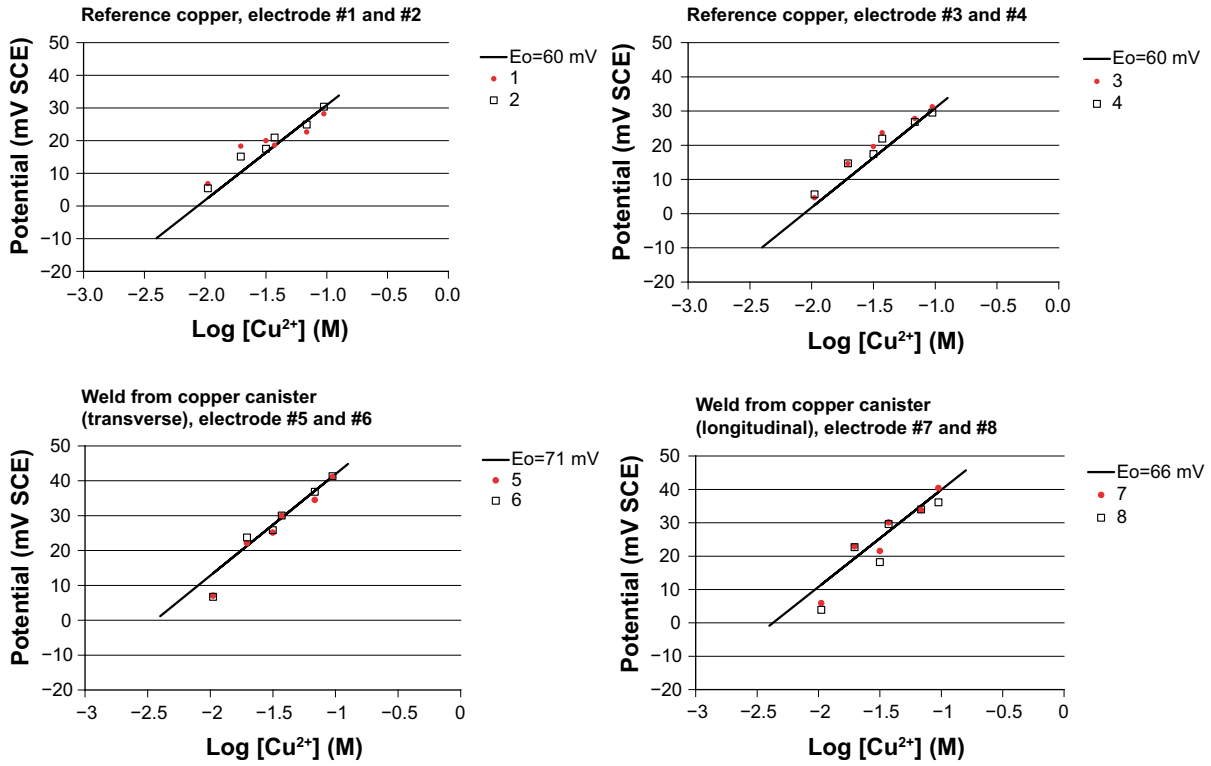

Figure 5-17. *Equilibrium potentials for copper electrodes #1−8 (reference and weld copper material) as function of the logarithm of the copper ion concentration. The solid lines have the theoretical slope of 29.1 mV per decade. The legend in each graph shows the value of the estimated* E_0.

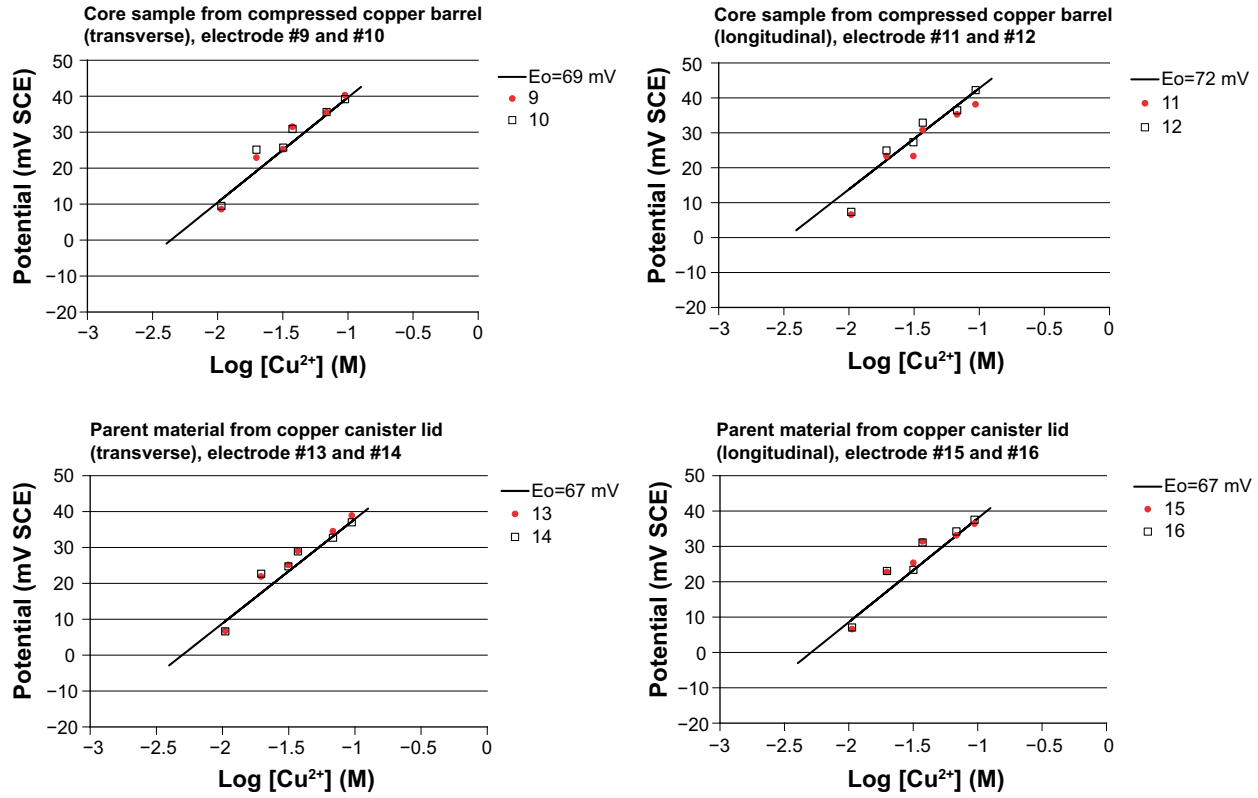

Figure 5-18. *Equilibrium potentials for copper electrodes #9−16 (core and parent copper material) as function of the logarithm of the copper ion concentration. The solid lines have the theoretical slope of 29.1 mV per decade. The legend in each graph shows the value of the estimated* E_0.

Table 5-5 summarizes the results for the copper materials from the copper weld, from the compressed barred and from the canister lid in terms of the estimated normal potentials, E_0.

Table 5-5. Summary of results from electrode potential measurements of copper from the weld, cold worked copper from compressed barrel, and copper from the canister lid.

Electrode Number	Orientation with respect to stress direction	Material	E_0 values from Run #3
1, 2	n/a	Reference copper	60
3, 4	n/a		60
5, 6	Transv	Weld	71
7, 8	Long		69
9, 10	Transv	Core	69
11, 12	Long		72
13, 14	Transv	Parent material, lid	67
15, 16	Long		67

Figures 5-17 and 5-18 show that some data points deviate from the straight line with almost 10 mV. In view of these deviations, the differences in E_0-values between the weld, the core and the parent material from the lid, in Table 5-5, are not considered significant.

5.2 Surface morphology after forced corrosion

One of the duplicate samples from the copper weld, from the compressed barred and from the canister lid were subjected to forced corrosion. After forced corrosion for 96 hours to a calculated average depth of attack of 0.04 mm, the electrodes were studied by confocal microscopy.

Figures 5-19 through 5-36 show microscopes image and depth profiles of the various copper samples. Figure 5-19 and Figure 5-22 show optical images of a small part of the electrode surface (2.6×2.6 mm) for the weld, for the two orientations. Figure 5-20 and 5-23 show depth profiles of the areas. The images are colour coded after the local depth of corrosion. The closest objects (peaks) are coded red and the most distant objects are coded blue. The images are composed of square arrays of data $1\,024 \times 1\,024$. Figures 5-21 and 5-24 show depth profiles along one direction for the weld specimens. Rows 200, 500 and 800 were selected, counting from the top of the depth profile images. The actual depth was calculated from the known average corrosion and applying this value as a row average. Figures 5-25 through 5-30 show the corresponding results for the cold worked compressed copper barrel, in the two orientations. Figures 5-31 through 5-36 show results for copper from the lid, in the two orientations studied.

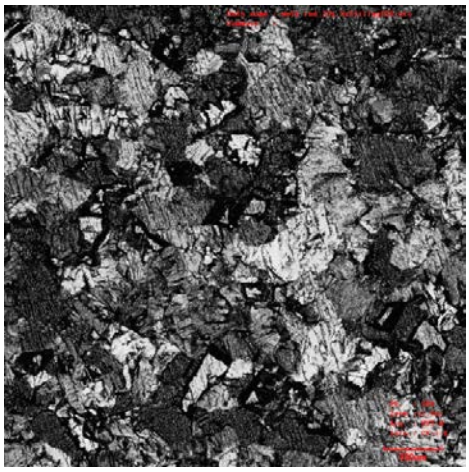

Figure 5-19. *Gray scale photograph of a part of the copper surface after forced corrosion to an average depth of 0.04 mm. Weld material (transverse) from copper canister lid. The imaged size is 2.6 × 2.6 mm.*

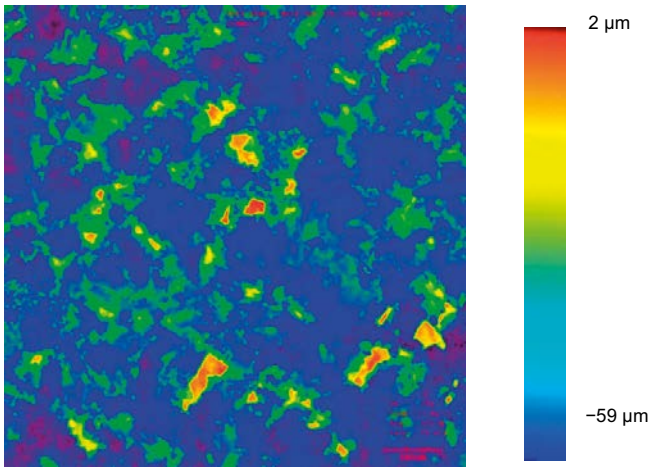

Figure 5-20. *Depth profile of a part of the copper surface after forced corrosion to an average depth of 0.04 mm. Weld material (transverse) from copper canister lid. The imaged size is 2.6 × 2.6 mm.*

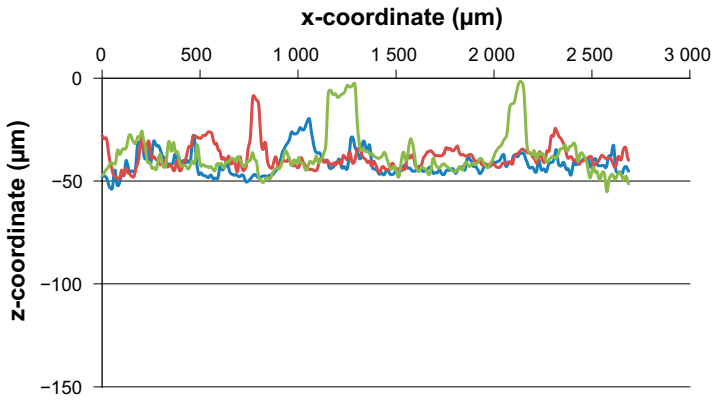

Figure 5-21. *Depth profile from the original surface of a part of the copper surface after forced corrosion to an average depth of 0.04 mm. The different lines represent different parallel lines across the surface in Figure 5-20. Weld material (transverse) from copper canister lid.*

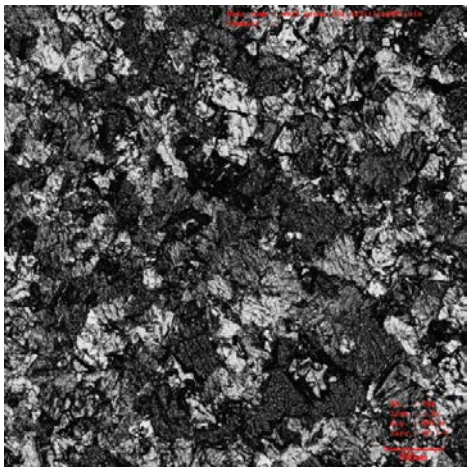

Figure 5-22. *Gray scale photograph of a part of the copper surface after forced corrosion to an average depth of 0.04 mm. Weld material (longitudinal) from copper canister lid. The imaged size is 2.6 × 2.6 mm.*

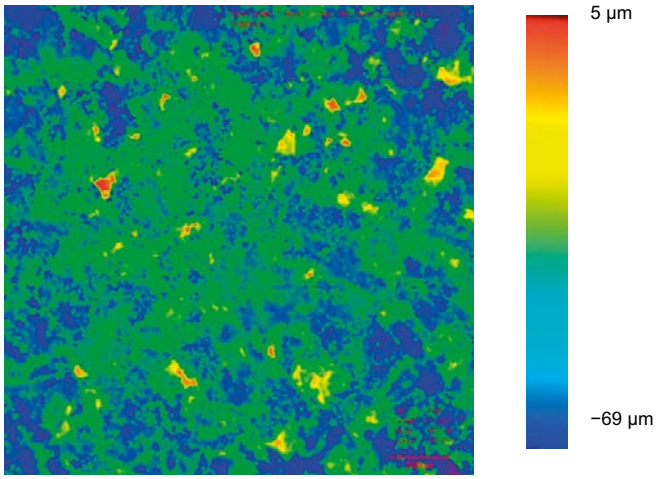

Figure 5-23. *Depth profile of a part of the copper surface after forced corrosion to an average depth of 0.04 mm. Weld material (longitudinal) from copper canister lid. The imaged size is 2.6 × 2.6 mm.*

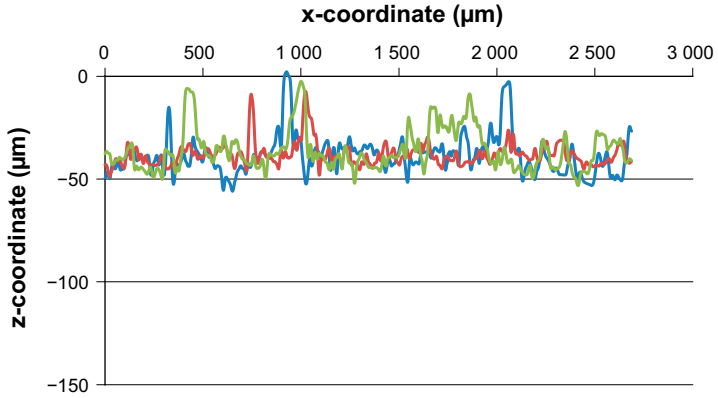

Figure 5-24. *Depth profile from the original surface of a part of the copper surface after forced corrosion to an average depth of 0.04 mm. The different lines represent different parallel lines across the surface in Figure 5-23. Weld material (longitudinal) from copper canister lid.*

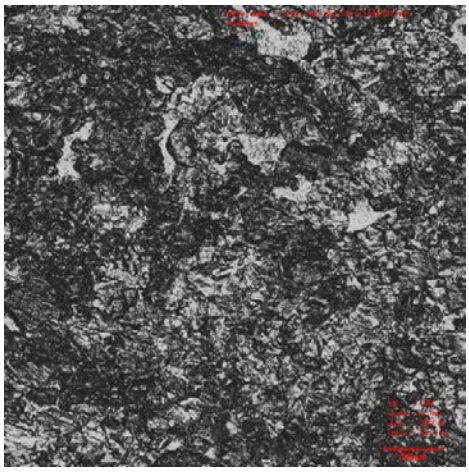

Figure 5-25. *Gray scale photograph of a part of the copper surface after forced corrosion to an average depth of 0.04 mm. Core material (transverse) from copper canister. The imaged size is 2.6 × 2.6 mm.*

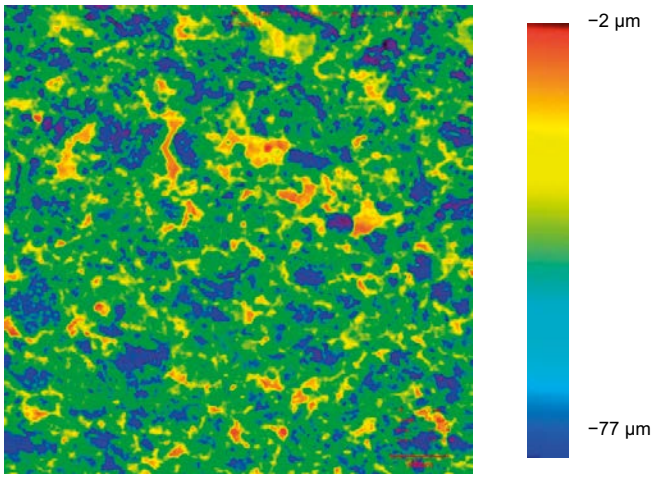

Figure 5-26. *Depth profile of a part of the copper surface after forced corrosion to an average depth of 0.04 mm. Core material (transverse) from copper canister. The imaged size is 2.6 × 2.6 mm.*

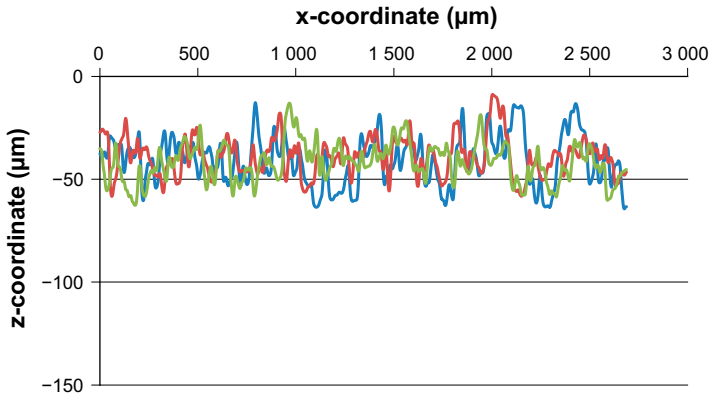

Figur 5-27. *Depth profile from the original surface of a part of the copper surface after forced corrosion to an average depth of 0.04 mm. The different lines represent different parallel lines across the surface in Figure 5-26. Core material (transverse) from copper canister.*

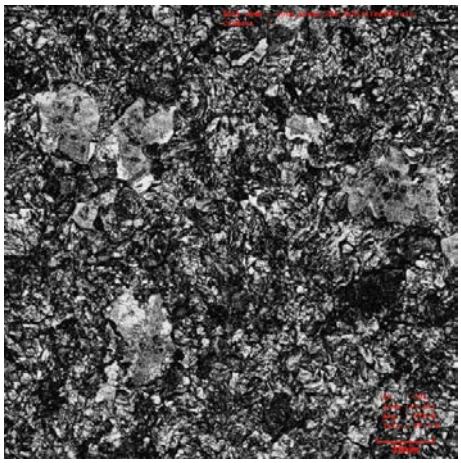

Figure 5-28. *Gray scale photograph of a part of the copper surface after forced corrosion to an average depth of 0.04 mm. Core material (longitudinal) from copper canister. The imaged size is 2.6 × 2.6 mm.*

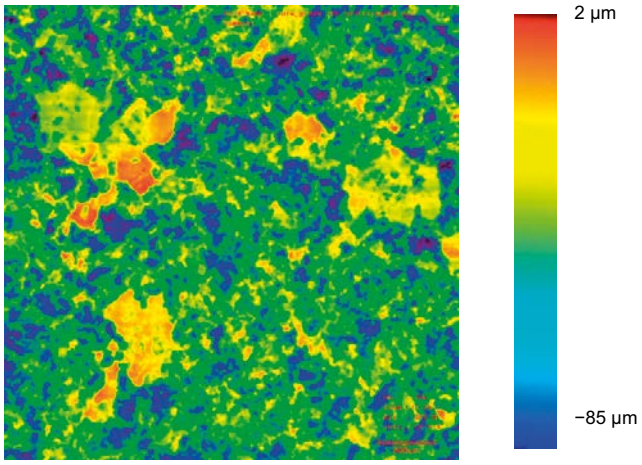

Figure 5-29. *Depth profile of a part of the copper surface after forced corrosion to an average depth of 0.04 mm. Core material (longitudinal) from copper canister. The imaged size is 2.6 × 2.6 mm.*

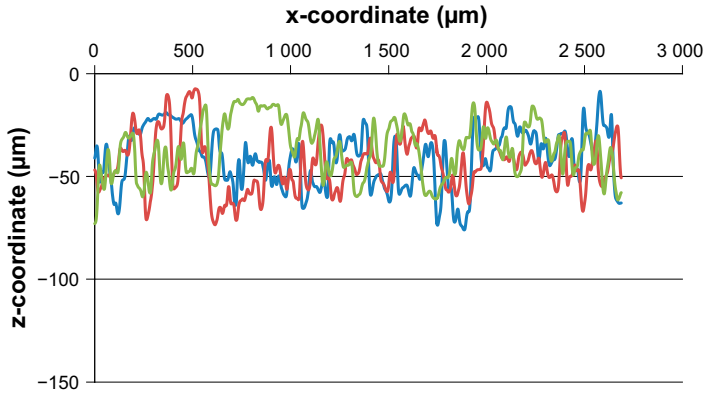

Figure 5-30. *Depth profile from the original surface of a part of the copper surface after forced corrosion to an average depth of 0.04 mm. The different lines represent different parallel lines across the surface in Figure 5-29. Core material (longitudinal) from copper canister.*

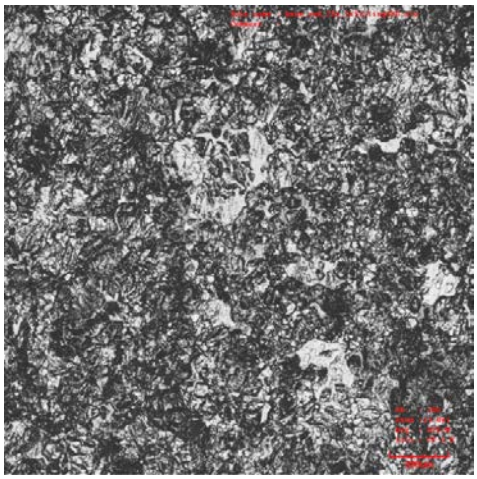

Figure 5-31. *Gray scale photograph of a part of the copper surface after forced corrosion to an average depth of 0.04 mm. Parent material (transverse) from copper canister lid. The imaged size is 2.6 × 2.6 mm.*

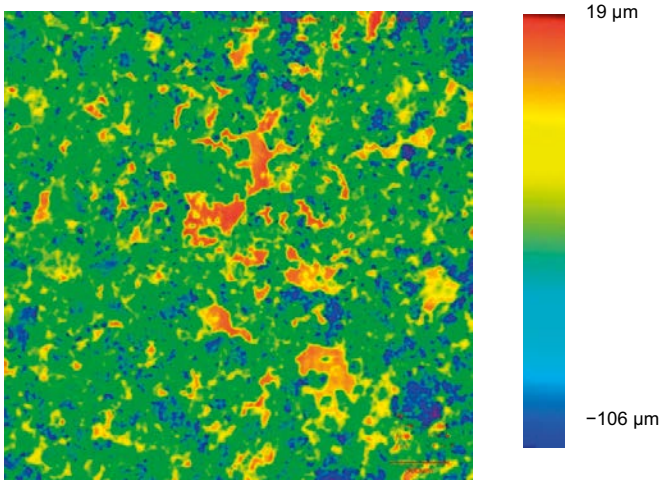

Figure 5-32. *Depth profile of a part of the copper surface after forced corrosion to an average depth of 0.04 mm. Parent material (transverse) from copper canister lid. The imaged size is 2.6 × 2.6 mm.*

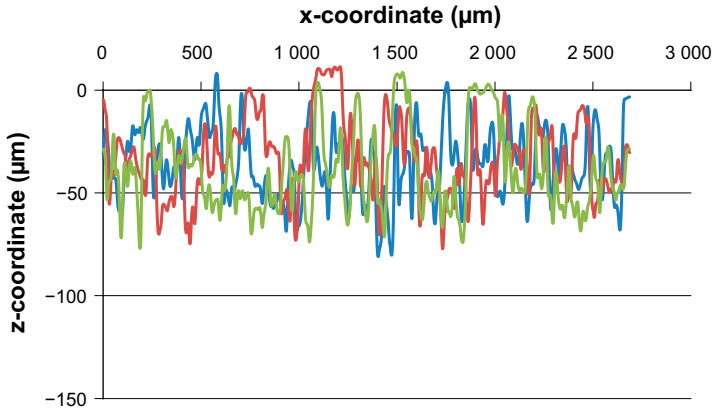

Figure 5-33. *Depth profile from the original surface of a part of the copper surface after forced corrosion to an average depth of 0.04 mm. The different lines represent different parallel lines across the surface in Figure 5-32. Parent material (transverse) from copper canister lid.*

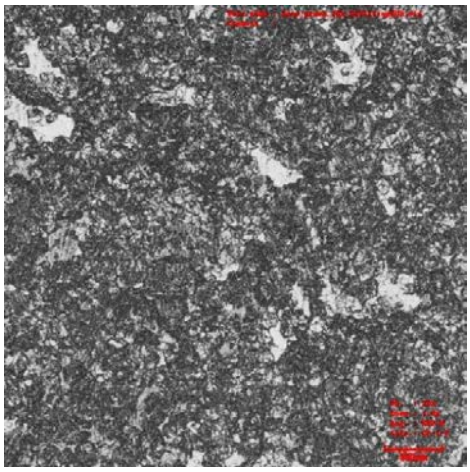

Figure 5-34. *Gray scale photograph of a part of the copper surface after forced corrosion to an average depth of 0.04 mm. Parent material (longitudinal) from copper canister lid. The imaged size is 2.6 × 2.6 mm.*

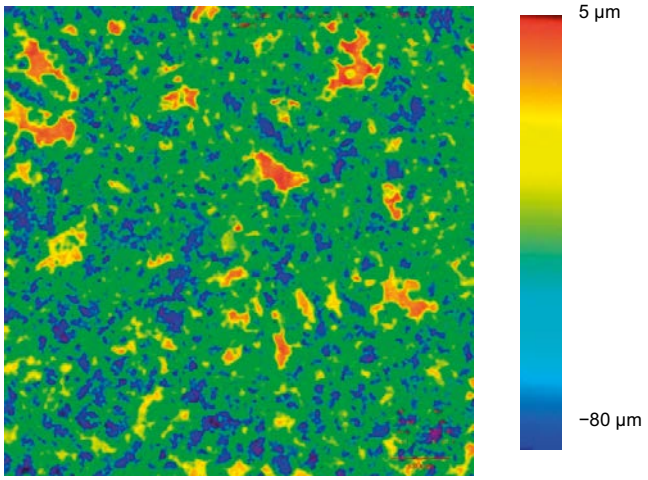

Figure 5-35. *Depth profile of a part of the copper surface after forced corrosion to an average depth of 0.04 mm. Parent material (longitudinal) from copper canister lid. The imaged size is 2.6 × 2.6 mm.*

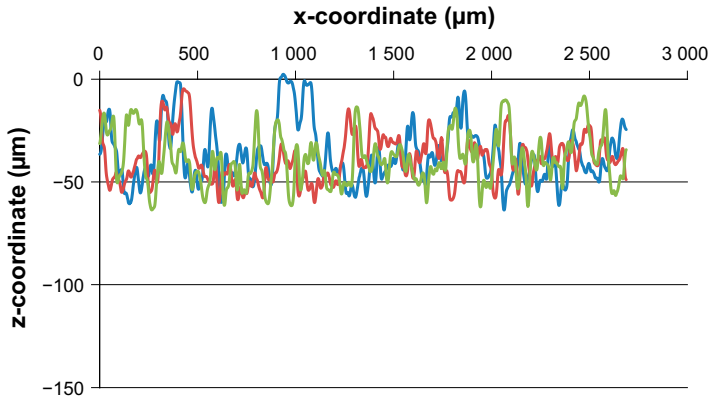

Figure 5-36. *Depth profile from the original surface of a part of the copper surface after forced corrosion to an average depth of 0.04 mm. The different lines represent different parallel lines across the surface in Figure 5-35. Parent material (longitudinal) from copper canister lid.*

5.3 Grain size distribution (optical microscopy)

Micrographs of the three different materials from test rods, in two different orientations, are shown in Figures 5-37 through 5-39.

For all specimens, it proved difficult to quantify the grain size due to the shape of the grains. However, no apparent difference in grain shape or size was discerned between the longitudinal and transverse cross sections of the samples subjected to 12 % and 15 % compressive strain. For the sample subjected to 12 % tensile strain, there appeared to be some elongation of the grains along one direction in the transverse cross section in comparison to the grain morphology in the longitudinal cross section. However, no evident variation in grain sizes was observed.

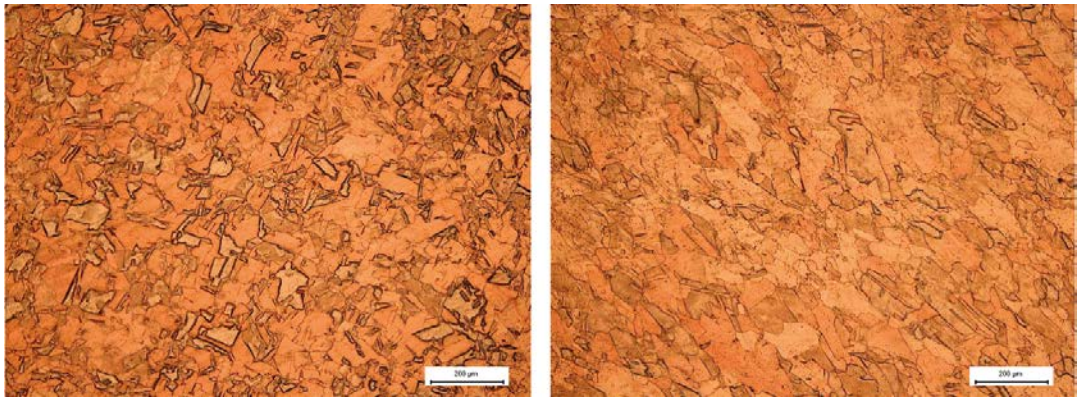

Figure 5-37. *Micrographs of copper electrode subjected to 12 % tensile strain. Images show the longitudinal, (left) and transverse (right) cross section with respect to the applied stress direction. 100 × magnification. Scale bars are 200 µm.*

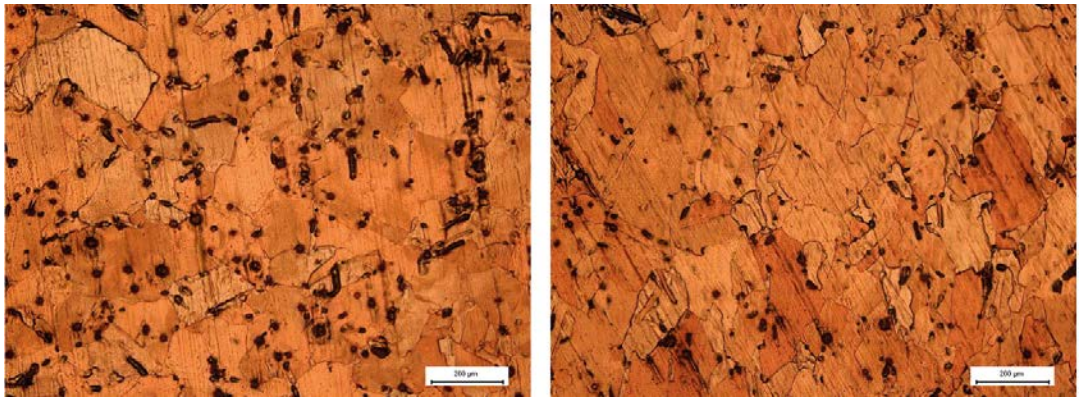

Figure 5-38. *Micrographs of copper electrode subjected to 12 % compressive strain. Images show the longitudinal (left) and transverse (right) cross section with respect to the applied stress direction. 100 × magnification. Scale bars are 200 µm. The black spots show remains of corrosion products from the etching procedure employed to reveal the microstructure.*

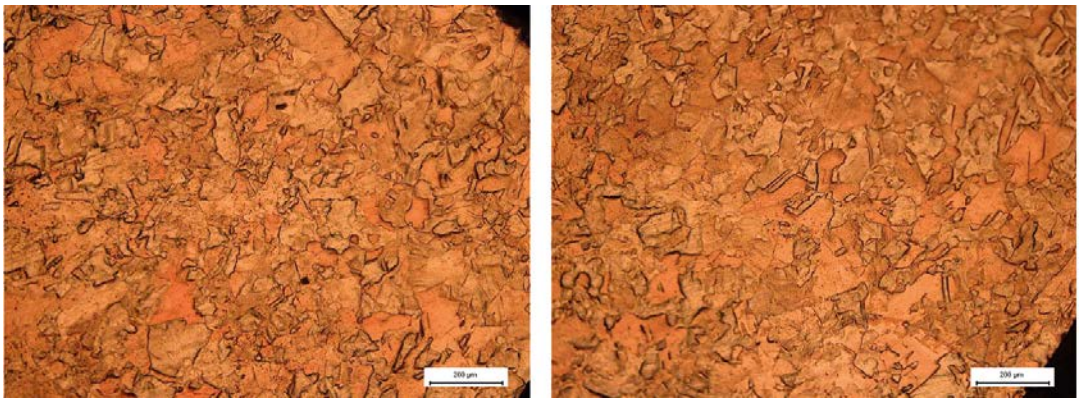

Figure 5-39. *Micrographs of copper electrode subjected to 15 % compressive strain. Images show the longitudinal (left) and transverse (right) cross section with respect to the applied stress direction. 100 × magnification. Scale bars are 200 µm.*

6 Discussion

6.1 Electrochemical nobility of the copper materials

All electrochemical measurements presented in this report were associated with an unusually high noise level. The experimental setup will apparently have to be shielded better against electro-magnetic noise, for future experiments.

The electrode potentials, for the tested materials, in Tables 5-1, 5-2 and 5-4 are generally more noble than the potentials for the reference material. This is illustrated in Figures 5-3, 5-4, 5-9, 5-10, 5-15 and 5-16, with a minimum of interpretation of data. The estimation of normal potentials requires that the potentials are interpreted as equilibrium values and that Nernst's equation is applicable. Table 5-3 quantifies how much more noble the tested materials are relative to the reference material, in terms of normal potentials.

The trends between run #1 and run #2 are different. The reference copper behaved as more noble in run #1 than in run #2. All the tested materials behaved less noble in run #1 than in run #2. A likely cause for this difference may be found in the treatment of the electrodes before each run. When run #1 was started the tested materials were freshly polished but the reference copper was not. When run #2 was started the tested materials were not repolished but the reference electrodes were. It would seem that previous exposure to the test solution followed by air exposure causes the normal potential to shift in the noble direction by a few mV. This may have several causes. Traces of surface oxides on the surface may cause the surface to behave as more noble or the least stable fractions of the surface may have corroded away during the first exposure so that the potential is determined more by the more stable, more noble, fractions of surface.

Tables 5-3 and 5-5 show that there is no significant influence of cold work on the apparent nobility of the material. The estimated values of the normal potential are the same independently of whether the strain was compressive or tensile. The estimated values are the same independently of the orientation of the surface in relation to the strain.

Table 5-5 shows that there are small differences in apparent nobility between the weld and the parent material in the lid. The samples from the weld appeared as slightly more noble than the lid and equal to that of cold worked copper from the compressed barrel. Gubner and Andersson found small differences in the corrosion potential between weld and parent material (Gubner and Andersson 2007). The present work adds to their observation and shows that very similar potentials are established at weld and parent material over a relatively wide range of equilibrium potentials.

The cold worked material tested as pieces from test rods in run #1 and run #2 (12 % compressive strain) originates from the same compressed copper barrel as the cold worked copper in run #3. The results, however, differ by about 10 mV. All results in Table 5-3, for runs #1 and #2, are about 10 mV higher than the results in Table 5-5, for run #3. The reason for this difference is not clear.

6.2 Surface morphology after forced corrosion

The microscope images and depth profiles in Figures 5-19 through 5-36 do not show any significant difference in surface morphology after corrosion to an average depth of 40 µm. Some areas seem almost uncorroded so that the location of the local surface is the same as it was before the forced corrosion. This behaviour is observed for all tested copper materials but is perhaps most apparent for the samples from the canister lid in Figures 5-33 and 5-36. No effects of the orientation of the exposed surface in relation to cold work or weld can be seen for any material. Also, no tendency to preferential corrosion at particular sites can be discerned. The maximum corrosion depth is about 60–70 µm. The positive values that appear are obviously artefacts.

6.3 Grain size distribution in cold worked copper from test rods

The material from the test rod subjected to 12 % compressive strain seems to have slightly larger grains than both the material from the test rod subjected to 15 % compressive strain and material from the test rod subjected to 12 % tensile strain. A slight elongation of the grains in the transverse surface of the material from the test rod subjected to 12 % tensile strain is discerned in the right hand image in Figure 5-37.

7 Conclusions

Cold worked, phosphorous doped copper has been studied electrochemically. The material studied behaved as more noble than beads of high purity copper. Material from a friction stir weld was similarly studied.

No significant influence of cold work on the apparent nobility of the material was found. The estimated values of the normal potential are the same independently of whether the strain was compressive or tensile. The estimated values are the same independently of the orientation of the exposed surface in relation to the strain.

The test does not reveal any significant differences in apparent nobility between the weld, the parent material from the lid and the cold worked copper.

When forced to corrode electrochemically to an average depth of 40 µm, some small areas of the 0.2 cm^2 electrodes seem completely uncorroded. No areas where the corrosion had concentrated to more than double the average depth were found.

References

SKB's (Svensk Kärnbränslehantering AB) publications can be found at www.skb.com/publications.

Andersson-Östling H C M, Sandström R, 2009. Survey of creep properties of copper intended for nuclear waste disposal. SKB TR-09-32, Svensk Kärnbränslehantering AB.

Gubner R, Andersson U, 2007. Corrosion resistance of copper canister weld material. SKB TR-07-07, Svensk Kärnbränslehantering AB.

SKB, 2010. Design, production and initial state of the canister. SKB TR-10-14, Svensk Kärnbränslehantering AB.

Taxén C, Sparr M, 2014. Corrosion properties of copper materials. SKB R-14-15, Svensk Kärnbränslehantering AB.

Wu R, Pettersson N, Martinsson Å, Sandström R, 2014. Cell structure in cold worked and creep deformed phosphorus alloyed copper. Materials Characterization 90, 21–30.

Arkitektkopia AB, Bromma, 2017

SKB is responsible for managing spent nuclear fuel and radioactive waste produced by the Swedish nuclear power plants such that man and the environment are protected in the near and distant future.

skb.se